Asparagine availability controls B cell homeostasis

Yavuz F. Yazicioglu[1,5], Eros Marin[1,5],
Karolina Bentkowska[1,6], Hana Andrew[1,6],
Robert Mitchell[1],
Zhi Yi Wong[1],
Joannah Fergusson[1],
Mohammad Ali[2,3],
Barbara Kronsteiner[2,3],
Mark Coles[1]
Christopher D. Buckley[1],
Susanna J. Dunachie[2,3,4],
Alexander J. Clarke[1,7]

1. Kennedy Institute of Rheumatology, University of Oxford, Oxford, UK
2. Nuffield Department of Medicine Centre For Global Health Research, Nuffield Department of Clinical Medicine, University of Oxford, Oxford, UK
3. Mahidol-Oxford Tropical Medicine Research Unit, Mahidol University, Bangkok, Thailand
4. National Institute for Health and Care Research Oxford Biomedical Research Centre, Oxford University Hospitals NHS Foundation Trust, Oxford, UK.

[5] Contributed equally
[6] Contributed equally
[7] Corresponding author (alexander.clarke@kennedy.ox.ac.uk)

Abstract

Germinal centre (GC) B cells proliferate at some of the highest rates of any mammalian cell, yet the metabolic processes which enable this are poorly understood. We performed integrated metabolomic and transcriptomic profiling of GC B cells, and found that metabolism of the non-essential amino acid asparagine (Asn) was highly upregulated. Asn was conditionally essential to B cells, and its synthetic enzyme, asparagine synthetase (ASNS) was markedly upregulated following their activation, through the integrated stress response sensor general control non-derepressible 2 (GCN2). When *Asns* is deleted, GC formation, and B cell survival in low Asn conditions were severely impaired, and removal of environmental Asn by asparaginase or dietary restriction markedly compromised the GC reaction. Using stable isotope tracing, we found that metabolic adaptation to the absence of Asn requires ASNS, and that oxidative phosphorylation, mitochondrial homeostasis, and synthesis of nucleotides was particularly sensitive to Asn deprivation. Altogether, we reveal that Asn metabolism acts as a key regulator of B cell function and GC homeostasis.

Introduction

The germinal centre (GC) reaction is essential for effective humoral immunity[1]. Following encounter with antigen, B cells organise in secondary lymphoid tissue and enter the GC reaction, a cyclic process in which somatic hypermutation (SHM) in a microanatomic region known as the dark zone (DZ) leads to random mutation of immunoglobulin genes. B cells then compete to interact with and receive help from T follicular helper cells in the microanatomic light zone (LZ). This process continues as affinity maturation occurs and memory B cells or plasma cells are generated.

GC B cells have some of the highest proliferation rates of all mammalian cells, yet their metabolism is unusual and incompletely understood[2]. Unlike most rapidly dividing immune cells, GC B cells predominantly use fatty acid oxidation and OxPhos rather than glycolysis[3–7], despite residing in a hypoxic and poorly vascularised micro-environment[8]. The key metabolic pathways that are important in their homeostasis have not been fully defined.

Amino acid availability is a critical regulator of T cell responses, demonstrated either by alteration of environmental abundance, synthesis, or interference with cellular import through solute transporters[9–15]. Amino acids are fundamentally required for protein synthesis, but are central to other metabolic processes[16], and it is apparent in T cells that availability of specific amino acids can have profound effects on their homeostasis.

In contrast, although it is known that B cell-derived lymphomas are sensitive to amino acid deprivation[17–20], and whilst loss of the capacity to synthesise serine, or deletion of CD98, a component of large neutral amino acid transporters, impairs GC formation, the importance of amino acid availability more broadly in B cell metabolism and humoral immunity is poorly understood[21].

Here, we find that GC B cells have high levels of amino acid uptake and protein synthesis in vivo. Using integrated multiomic analysis we identify asparagine (Asn), a non-essential amino acid, as a critical regulator of B cell homeostasis and GC formation. Mice with conditional deletion of asparagine synthetase (ASNS) in B cells have selective impairment of GC formation, and depletion of environmental Asn strongly suppresses the GC reaction. ASNS is regulated by sensing through the integrated stress response, and whilst most Asn in B cells is obtained from the extracellular environment following activation, mechanistically, loss of ASNS leads to profound metabolic dysfunction characterised by impairment of OxPhos and failure of nucleotide synthesis, which can be rescued by nucleotide supplementation.

Results

GC B cells have highly active protein synthesis

To evaluate protein synthesis rates in GC B cells, we immunised mice with sheep red blood cells (SRBC) and first examined expression of CD98, which forms heterodimers with the amino acid transporter protein SLC7A5 to form L-type amino acid transporter 1 (LAT1), at day 9 following immunisation. As previously reported, CD98 was markedly upregulated in GC B cells compared with IgD$^+$ naïve B cells (Fig. 1A-B)[21], suggesting high amino acid uptake. To more directly estimate protein synthesis rates in GC B cells in vivo and in their spatial context, we used bio-orthogonal non-canonical amino acid tagging (BONCAT), with the amino acid analogues L-azidohomoalanine (L-AHA), and O-propargyl-puromycin (OPP) visualised in situ using Click chemistry[22]. OPP is a puromycin analogue which enters the acceptor site of ribosomes and is incorporated into nascent proteins. L-AHA is a methionine analogue, which does not lead to ribosomal stalling once included in polypeptides. To label GC B cells, we immunised mice expressing Rosa26^{STOP}tdTomato under the control of *Aicda-Cre*, with SRBC. At day 14, we first injected a pulse of L-AHA and then after four hours a pulse of OPP, sacrificing mice one hour later (Fig. 1C). We then used Click chemistry to label splenic sections. We found that incorporation of L-AHA and OPP were markedly upregulated in the GC compared with the surrounding follicle of naïve B cells, indicating highly active protein synthesis (Fig. 1D, Extended Data Fig. 1A). We also labelled GC B cells with OPP ex vivo, and quantified its incorporation by flow cytometry (Fig. 1E). This confirmed a significant increase in OPP signal in GC B cells compared with naïve IgD$^+$ B cells. Within

the GC B cell population, signal was highest in dark zone (CXCR4^{hi} CD86^{low}) GC B cells, which are undergoing proliferation and SHM (Fig. 1E). GC B cells therefore have high rates of both amino acid transporter expression and protein synthesis.

Asparagine metabolism is upregulated in GC B cells

We next directly profiled the metabolite content of GC B cells. To do so, we isolated GC and naïve B cells from pools of wild type mice following immunisation with SRBC and quantified key metabolites using liquid chromatography-mass spectrometry (LC-MS) (Fig. 2A). This revealed a broad increase in the levels of metabolites in GC B cells, with overrepresentation of intermediates of glycolysis, the TCA cycle, and most amino acids (Fig. 2B). Notably however, nucleotide precursor molecules were depleted in GC B cells, potentially reflective of their consumption during the nucleic acid synthesis required for high rates of proliferation. To refine our approach, we fused metabolite and transcriptional datasets[23] and performed integrated pathway analysis on the combined data using hypergeometric set testing (Fig. 2C). We found that there was enrichment of amino acid metabolic pathways in GC B cells, most notably the Kyoto Encyclopedia of Genes and Genomes (KEGG) Alanine, Aspartate, and Glutamate (AAG) metabolism pathway. Examination of the leading-edge genes of the AAG pathway in an independent transcriptional dataset revealed an approximately 40-fold increase in the expression of asparagine synthetase (*Asns*) and a 15-fold increase in glutamic oxaloacetic transaminase-2 (*Got2*) in GC B cells compared with naïve follicular B cells (Fig. 2D)[24]. We confirmed upregulation of *Asns* and *Got2* in sorted GC B cells by qPCR (Fig. 2E).

ASNS synthesises Asn from aspartate (Asp) in an ATP-dependent reaction, and GOT2 synthesises Asp from the TCA cycle intermediate oxaloacetate[25] (Fig. 2F). The levels of both Asn and Asp were markedly increased in GC compared with naïve B cells, which had equivalent glutamate (Glu) levels (Fig. 2G). To examine ASNS expression in its spatial context, we performed multiplex imaging of human tonsils (Fig. 2H). ASNS was strongly expressed in GCs and MZB1^{+} plasmablasts. There was negligible expression in the IgD^{+} B cell follicle or in the CD3^{+} T cell zone. ASNS levels were spatially regulated within the GC, with higher expression in the DZ, where proliferation and SHM occurs (Extended Data Fig. 2A,B). Asn metabolism is therefore one of the most upregulated pathways in GC B cells and plasmablasts, suggesting that it may play an important role in their homeostasis.

***Asns* is selectively required by GC B cells**

To determine if Asn synthesis is required for B cell development or GC formation, we conditionally deleted *Asns* under the control of *Cd79a-Cre* (B-Asns hereafter)(Extended Data Fig. 3A), which is active at the earliest stages of B cell development[26]. Whilst B cell development in the bone marrow and periphery was intact in B-Asns mice (Extended Data Fig. 3B-D), following immunisation with SRBCs, splenic GC B cells were significantly reduced proportionately and numerically at day 9 (Fig. 3A-B). There was an increase in the ratio of GC B cells with DZ to LZ markers in B-Asns mice (Fig. 3C). The CXCR5^{+}PD-1^{hi} T_{FH} compartment was unaltered (Extended Data Fig. 3E). GC B cells from intestinal Peyer's patches (PP), which harbour chronic GCs reactive against intestinal antigens, were also significantly decreased in B-Asns mice (Fig. 3D). Surprisingly, there were no differences in the proportions of splenic plasma cells (Fig. 3E) and total immunoglobulin levels at steady state were comparable (Extended Data Fig. 3F). Following subcutaneous immunisation with 4-hydroxy-3-nitrophenylacetyl-chicken gamma globulin (NP-CGG) in alum, at day 14 while the total GC B cell numbers in the draining lymph node were significantly lower in B-Asns,

the numbers of NP-binding GC B cells did not differ significantly (Extended Data Fig. 3G), nor did serum anti-NP antibody levels (Extended Data Fig. 3H).

Next, we performed transcriptional profiling of B-Asns and B-WT GC B cells, following immunisation with SRBC (Fig. 3F). Using gene set enrichment analysis, we found upregulation of pathways associated with the endoplasmic reticulum (ER) stress response to misfolded proteins, and downregulation of B cell activation gene sets, in keeping with potentially defective cellular interactions associated with abnormal DZ/LZ partitioning.

We then determined whether reduction in environmental Asn supply affected GC B cell formation. To minimise confounding due to e.g. cage effects or food intake, we first generated mixed chimeras with CD45.1 wild type and CD45.2 B-Asns or B-WT bone marrow. After 8 weeks, mice were given either an Asn-free or normal diet for 12 days, immunised with SRBC, and analysed after a further 9 days of dietary modification (Fig. 3G). Although we had not observed a difference in B cell development in the resting state in B-Asns mice, in the chimeric setting there was a modest reduction in the proportion of CD45.2 B cells (Extended Data Fig. 3I-J), which was seen with both diets. However, the relative proportion of GC B cells in CD45.2 B-Asns B cells was much lower in mice fed an Asn-free diet, and the DZ/LZ ratio was reversed (Fig. 3H-J). Also reduced were splenic plasma cells of B-Asns origin (Fig. 3K). Interestingly and unlike the non-chimeric setting, we did not observe a difference in B-Asns GC B cell proportions in mice fed the control diet. This suggests that the defect we observed in B-Asns mice may be partially non-B cell-intrinsic.

We then treated mice with asparaginase (ASNase), an enzyme of bacterial origin which rapidly and effectively hydrolyses Asn and is a well-established treatment for leukaemia. We immunised mice with SRBC, and then administered ASNase every two days over a nine day period before analysis (Fig. 3L). There was a marked reduction in GC B cell formation in treated mice (Fig. 3M).

Loss of *Asns* in B cells therefore specifically disrupts the GC reaction, seen to a greater extent with dietary Asn restriction, and is associated with activation of ER stress transcriptional programs.

Asn controls B cell homeostasis

Asn is a non-essential amino acid and can be either acquired exogenously or synthesised by ASNS. To understand the dynamics of Asn uptake following B cell activation, we first stimulated wild type B cells in vitro with either the TLR9 agonist CpG and agonistic anti-CD40 antibody, or IL-4 and agonistic anti-CD40, for 24h in the presence of ^{15}N-labelled Asn, and quantified amino acids by mass spectrometry. We found a generalised increase in the intracellular concentrations of most amino acids, but in particular proline (Pro), glutamate (Glu), and Asn (Fig. 4A). The majority of Asn was labelled with ^{15}N in all conditions, indicating high exogenous uptake, and in preference to endogenous synthesis, which is bioenergetically demanding (Fig. 4B).

Next, to determine the requirements of B cells for exogenous Asn, we stimulated them with agonistic anti-CD40 and IL-4 in RPMI-1640 media with varying concentrations of Asn. Standard RPMI-1640 contains supraphysiologic concentrations of Asn (378μM) compared with those found in plasma (~40μM) and cerebrospinal fluid (CSF) (~4μM)[27,28]. We found that Asn was conditionally essential for B cell viability and proliferation, determined by stimulus and the time point at which Asn was removed. When B cells were deprived of Asn or supplemented with a low concentration of Asn (4μM), and stimulated with IL-4 and anti-

CD40 for 72h, there was a severe reduction in cell viability and proliferation, compared with supplementation of Asn at 40µM or 400µM concentrations (Fig. 4C-D). We noted no decrease in cell proliferation or viability on withdrawal of exogenous aspartate (Asp) and/or Glu, although glutamine (Gln) was required for B cell survival as previously described[29] (Fig. 4E and Extended Data Fig. 4A). There was a reduction in the expression of the activation markers CD86 and MHCII following Asn deprivation, nascent protein synthesis measured by OPP incorporation was lower at 24h (Extended Data Fig. 4B-D), and apoptosis was increased (Extended Data Fig. 4E).

However, when B cells were stimulated with IL-4 and agonistic anti-CD40 with Asn for 72h and then subsequently deprived of Asn for a further 24h, there were minimal differences in survival, but proliferation and OPP incorporation were slightly reduced (Fig. 4F and Extended Data Fig. 4F). This indicates that exogenous Asn is essential for survival and cell division in the early stages of B cell activation, but becomes less important later. The capacity of B cells to survive without Asn is therefore both time and stimulus dependent.

To understand if this may be mediated by acquisition of the capacity to synthesise Asn, we next examined the kinetics of ASNS expression. Transcription of *Asns* and expression of ASNS protein steadily increased following stimulation with IL-4 and agonistic anti-CD40 (Fig. 4G-H). When Asn was excluded from media, *Asns* transcription and protein abundance were significantly upregulated. We found there was synergistic upregulation of ASNS when B cells were stimulated with both IL-4 and agonistic anti-CD40 (Fig. 4I).

Survival, proliferation, and activation of B-Asns B cells were severely compromised when Asn was absent but normal when Asn was present (Fig. 4J, Extended Data Fig. 4G). When B-Asns B cells were pre-stimulated in the presence of Asn, which was then withdrawn, the previously demonstrated protective effect of activation was attenuated (Fig 4K). Plasmablast differentiation induced by LPS and IL-4 was completely abolished in B-Asns B cells when Asn was absent or at low concentrations (10µM), but remained unchanged in the presence of Asn (Fig. 4L).

In vitro culture systems lack the spatial organisation and cellular complexity of lymphoid tissue, and may therefore reproduce normal immune dynamics less well. We used a live ex vivo lymph node slice platform to investigate how Asn deprivation affected GC B cells from immunised mice[30]. We found that GC B cells from B-Asns lymph nodes were much reduced after 24h of culture without Asn, and the proportion of IgD^+ and therefore non-activated B cells was higher. T cell proportions were unaffected (Extended Data Fig. 4H).

Asn uptake and synthesis is therefore specifically required during initial B cell activation, and loss of synthetic capacity leads to severely compromised cell division and survival in B cells in low Asn conditions.

The integrated stress response regulates B cell function through ASNS

Asns is known to be upregulated following activation of the integrated stress response (ISR), which occurs as a consequence of a variety of cellular stressors, including amino acid withdrawal[31,32]. A key event in the ISR is the phosphorylation of elongation initiation factor 2 alpha (eIF2α) by the kinase general control non-repressible-2 (GCN2). Phosphorylated eIF2α then controls transcription and translation of the ISR effector molecules activating transcription factor-4 (ATF4) and C/EBP homologous protein (CHOP)(Fig. 5A).

We observed elevated levels of p-eIF2α and ASNS in sorted GC B cells, suggestive of ISR activation (Fig. 5B). We then examined the temporal dynamics of eIF2α phosphorylation in B cells, and found that p-eIF2α was increased at 6 hours following stimulation with IL-4 and agonistic anti-CD40 in the absence of Asn (Fig. 5C). *Atf4* transcription and protein abundance were elevated with Asn deprivation, and this effect was significantly enhanced in B-Asns B cells (Fig. 5D-E). We observed a reduction in mTORC1 activation assessed by phosphorylation of 4E-BP1 when B cells were stimulated without Asn, which was more pronounced in those from B-Asns mice (Fig. 5E).

To directly assess the importance of the GCN2-mediated ISR in Asn synthesis, we next examined *Gcn2*$^{-/-}$ B cells. *Gcn2*$^{-/-}$ B cells were unable to upregulate either ATF4 or ASNS following stimulation (Fig. 5E-F), an effect seen even in Asn-replete conditions. *Asns* has also been reported to be under distinct regulation by *Zbtb1*[33], but we did not observe its upregulation in B cells following Asn deprivation (Extended Data Fig. 5A).

To understand the functional consequences of GCN2 activity, we measured the level of CHOP by flow cytometry, and found that it was significantly upregulated in GC B cells compared to IgD^{+} naïve B cells (Fig. 5G). CHOP was highly expressed in B-Asns B cells deprived of Asn, and to a lesser extent in B-WT B cells, following in vitro activation with IL-4 and agonistic anti-CD40 (Fig. 5H).

We also observed that survival was reduced in *Gcn2*$^{-/-}$ B cells stimulated with agonistic anti-CD40 and IL-4 in the absence of Asn, although paradoxically to a lesser extent than those from wild type mice (Fig. 5I). However, proliferation and activation measured by IgD downregulation were severely reduced, resembling the phenotype of Asn-deprived B-Asns B cells (Fig. 5J-K). Additionally, we observed defective plasmablast differentiation induced by LPS and IL-4 in Asn-deprived *Gcn2*$^{-/-}$ B cells (Fig. 5L).

Given the dependence on the ISR for B cells to survive Asn deprivation, we then asked if its additional activation might rescue the defects seen in the absence of Asn. We treated B cells with the GCN2 activator halofuginone[34], and found that even when Asn was present, very low concentrations led to decreased survival and B cell activation (Fig. 5M-N). This suggested that the extent of the ISR was carefully balanced in activated B cells, and excessive ISR activation was harmful. The GCN2 branch of the ISR is therefore essential for ASNS expression and cellular homeostasis in B cells.

Disruption of asparagine availability alters B cell metabolism

To understand how Asn withdrawal affects B cell metabolism, we performed stable isotope resolved LC-MS on B cells from B-WT or B-Asns mice, stimulated for 72h in Asn-replete media, before switching for 24h into media with or without Asn, and [U-^{13}C]-glutamine, or $^{15}N_1$-glutamine, labelled at either the amine or amide nitrogen position (Fig. 6A). Since ASNS transfers the amide nitrogen group of glutamine to that of asparagine (acting as an amidotransferase), positional labelling can provide information on ASNS activity[25].

Intracellular Asn levels were greatly reduced in Asn-deprived conditions in both B-WT and B-Asns B cells, confirming our previous observation that exogenous uptake is dominant, but to significantly greater degree in those from B-Asns mice (Fig. 6B). B-WT cells did not engage in significant Asn synthesis when Asn was present, with negligible labelling of Asn with Gln-derived ^{15}N from either the amino or amide position (Fig 6C-D). Following Asn deprivation, around half of the intracellular Asn pool was ^{15}N-labelled in B-WT B cells, reflecting de novo synthesis by ASNS. As expected, B-Asns B cells were incapable of Asn

synthesis and no Asn was ^{15}N labelled. There was minimal labelling of Asn from ^{13}C glutamine, but around a quarter of Asp was labelled, with no difference between B-WT and B-Asns B cells, suggesting very little of the Gln-derived Asp pool was diverted to Asn synthesis (Fig. 6E, Extended Data Fig. 6A).

In B-WT cells, Asn deprivation had subtle effects on metabolite relative abundance, but significantly reduced fractional labelling from [U-^{13}C]-glutamine and $^{15}N_1$-glutamine. Despite small differences in intracellular Asn, B-Asns B cells exhibited profound metabolic dysfunction upon Asn withdrawal, with large reductions in metabolite relative amounts and glutamine-derived ^{15}N incorporation (Fig. 6F).

We next performed pathway analysis to systemically describe these results. Comparing B-WT and B-Asns B cells, both deprived of Asn, there were a common set of significantly different pathways (Fig. 6G), including AAG, tRNA biosynthesis, glutathione synthesis, sphingolipid metabolism and glyoxylate. We noted that B-Asns B cells, when deprived of Asn, substantially downregulated metabolites in the TCA cycle, nucleotide biosynthesis. pentose phosphate pathway, and β-alanine metabolic pathways (Fig. 6G). Asn is therefore essential to regulate metabolic homeostasis in B cells,

Mitochondrial function in B cells requires Asn

Given the abnormalities in TCA cycle metabolism we observed following Asn withdrawal, we next performed extracellular flux analysis to explore OxPhos and glycolysis in a dynamic setting. We found that Asn concentration was strongly associated with oxygen consumption rate (OCR) and extracellular acidification (ECAR), reflecting OxPhos and lactate production respectively (Fig. 7A-E, Extended Data Fig. 7A-B), and the deleterious effect of low Asn was more pronounced in B-Asns B cells (Fig 7C-D). In keeping with our metabolite profiling, this effect was only seen when Asn was limited. Surprisingly, the maximal respiration induced by the mitochondrial uncoupler carbonyl cyanide-p-trifluoromethoxyphenylhydrazone (FCCP) remained unchanged between B-WT and B-Asns B cells across all Asn concentrations, resulting in a significantly higher maximal-to-basal respiration ratio, known as the spare respiratory capacity (SRC), in B-Asns B cells (Fig. 7E, Extended Data Fig. 7B).

Supplementation with a cell-permeable analogue of the TCA cycle metabolite alpha-ketoglutarate (α-KG), dimethyl 2-oxoglutarate (DM-OG) has been reported to increase cell viability in T cells treated with L-asparaginase[35]. We therefore hypothesized that supplementation with DM-OG could potentially restore defective mitochondrial metabolism and improve B cell homeostasis in Asn-deficient conditions. However, DM-OG failed to rescue the defective B cell survival in B-WT and B-Asns B cells under Asn-free conditions (Extended Data Fig. 7C).

We next directly imaged mitochondria in B-WT and B-Asns B cells using 3D Lattice structured illumination microscopy (SIM) (Fig. 7F). Mitochondrial volume and count were not different when Asn was present, but were much reduced in the absence of Asn, and again this was seen to a greater extent in B-Asns B cells (Fig. 7G-H). This was reflected in reduced MitoTracker signal and mitochondrial reactive oxygen species production, measured by flow cytometry (Extended Data Fig. 7D-E)

B cells undergo profound mitochondrial remodelling upon activation associated with mitochondrial protein synthesis of electron transport chain (ETC) proteins[36]. Given the defective cytoplasmic protein translation we observed with Asn deprivation, we examined whether mitochondrial translation and ETC homeostasis was also affected. Flow cytometric

characterisation of the ETC complexes of wild type B cells stimulated without Asn revealed reduced levels of the mitochondrially-translated subunit COX I, relative to its neighbouring subunit COX IV, which is translated in the cytoplasm. However, the relative abundance of cytochrome C (Cyt C) which is encoded in the nucleus, remained unaltered, indicating a selective disruption of mitochondrially translated subunits (Fig. 7I).

Taken together, these findings indicate that Asn availability maintains mitochondrial ETC homeostasis, and ASNS regulates mitochondrial respiration in low Asn-conditions.

ASNS gates nucleotide synthesis in B cells

Mitochondrial function is intimately linked to nucleotide metabolism[37]. In our metabolomics dataset, we found that nucleotide synthesis pathways were selectively impaired in B-Asns B cells following Asn deprivation. Detailed metabolite pathway analysis revealed significant downregulation of intermediate metabolites in both de novo purine and pyrimidine biosynthesis branches (Fig. 8A). Downregulated in B-Asns B cells were orotate and uridine monophosphate (UMP), a common precursor of pyrimidine end-products cytosine and thymidine. We transcriptionally profiled key enzymes in the nucleotide synthesis pathway, and observed marked dysregulation when Asn was absent, which was more pronounced in B-Asns B cells (Fig. 8B).

The enzyme catalysing the oxidation of dihydroorotate to orotate is dihydroorotate dehydrogenase (DHODH), which is located in the mitochondria and forms a functional link between de novo pyrimidine biosynthesis and ETC activity[38,39]. We quantified DHODH levels and found it markedly reduced with Asn deprivation. Notably, B-Asns B cells had the lowest DHODH levels in the absence of Asn, consistent with their lower mitochondrial mass and significantly downregulated pyrimidine metabolites (Fig. 8C). Interestingly, 5-aminoimidazole-4-carboxamide ribonucleotide formyltransferase/IMP cyclohydrolase (ATIC), which is responsible for the synthesis of inosine monophosphate (IMP) in the de novo purine synthesis pathway was not altered at the protein level (Fig. 8C). Phosphorylated carbamoyl-phosphate synthetase 2, aspartate transcarbamylase, and dihydroorotase (CAD), the trifunctional enzyme upstream of DHODH was reduced in B-Asns B cells deprived of Asn (Fig. 8C).

Finally, we performed a rescue experiment by supplementing B-WT and B-Asns B cells with nucleosides including guanosine, adenosine, thymidine, cytidine, and uridine, which bypasses the activity of nucleotide biosynthetic enzymes, including DHODH and CAD.
In conditions of Asn restriction, nucleoside supplementation substantially increased viability in both B-WT and B-Asns B cells following 72h culture (Fig. 8D), but was unable to restore normal proliferative capacity (Fig. 8E). Importantly, nucleoside supplementation did not affect B cell viability or proliferation when Asn was unrestricted.

These data show that *Asns* therefore essential to regulate B cell metabolic homeostasis, and if it cannot be obtained in sufficient amounts from the environment or synthesised by ASNS, there is impairment of nucleotide biosynthesis.

Discussion

Here we show using integrated multiomics that Asn metabolism is upregulated in GC B cells and required for their homeostasis, and that deprivation of Asn either from the external environment or by loss of its synthesis strongly alters cellular metabolism, and in particular impairs OxPhos and nucleotide synthetic capacity.

We found that GC B cells exhibited high levels of protein synthesis in vivo, and highly expressed the amino acid transporter protein subunit CD98. This corresponded with a preference for uptake of extracellular Asn, which was greatly increased following cell activation. Initial stimulation in the presence of Asn provided a protective effect against subsequent Asn withdrawal, as has also been observed in $CD8^+$ T cells[40], which we found was mediated in part by upregulation of ASNS, which was almost undetectable in naïve B cells. Although the effects of amino acid uptake on T cells is increasingly well described[11,41], how this influences B cell biology is still poorly understood and requires further study.

Lack of Asn severely affected cellular metabolism in B cells, and in particular OxPhos. This was in striking contrast to reports in $CD8^+$ T cells[13,15], in which Asn deprivation leads to activation of OxPhos and increased nucleotide synthesis, associated with increased proliferative capacity and enlarged mitochondrial mass, although others have noted reduction of cell division without Asn in this cell type[12,14]. We found that Asn-deprivation led to a substantial drop in mitochondrial volume, and we observed that there was imbalance of expression of mitochondrially-encoded ETC proteins. It is unclear why B cells should be so much more vulnerable to the lack of Asn than $CD8^+$ T cells, but may reflect more profound cellular remodelling following activation, or other differences in core metabolism.

An important consideration in all studies of metabolism in vitro is how to approximate the concentrations of metabolites found within tissue. Whilst this has received attention in the context of the tumour microenvironment, very little is known about normal tissues and especially within complex structures like GCs. GCs are hypoxic and poorly vascularised, but local concentrations of Asn remain unclear. In our study we noted impaired B cell homeostasis at Asn concentrations below 10μM in vitro, which is intermediate between venous blood and CSF. Advances in mass spectrometry imaging may allow more accurate quantification of metabolites in their spatial context in the future[42].

A key finding from our work is that Asn availability acts to gate nucleotide synthesis in B cells. GC B cells have high rates of nucleic acid synthesis, in keeping with their active translational programming, and our LC-MS data revealed they had low levels of nucleotides, suggestive of their consumption. Analysis of Asn synthesis from glutamine showed that even following activation, which was associated with upregulation of ASNS, the great majority of Asn was exogenously acquired. Nonetheless ASNS was essential for metabolic homeostasis and nucleotide synthesis, despite seemingly modest rates of Asn synthesis. This raises the interesting question of whether ASNS might have other, non-synthetic functions, as has been recently demonstrated for the enzyme phosphoglycerate dehydrogenase (PHGDH), whose canonical function is to synthesise serine[43]. The relationship between amino acid availability and nucleotide synthesis has been previously defined through mTORC1 signalling, acting via phosphorylation of CAD, or the tetrahydrofolate cycle[44,45]. It is therefore possible that in GC B cells, Asn availability tunes these nucleoside synthetic pathways, either through mTORC1 or other mechanisms. An important node in B cell nucleoside metabolism downregulated with Asn deprivation involved enzymes which synthesise and oxidise dihydroorotate through CAD and DHODH. Interestingly, there was mismatch between enzyme transcription and abundance at the protein level for DHODH, which raises the possibility that translation of this protein is selectively affected by Asn deficiency. How the interplay of ATF4 activation by the ISR compared with mTORC1 in activated and Asn-deficient B cells is currently unclear.

ASNase has been a cornerstone of the treatment of leukaemia for decades, but given the results of our work, ASNS may also be a novel therapeutic target in non-malignant,

autoimmune disease mediated by the GC reaction, and is deserving of future study in this context.

Figures and legends

Figure 1

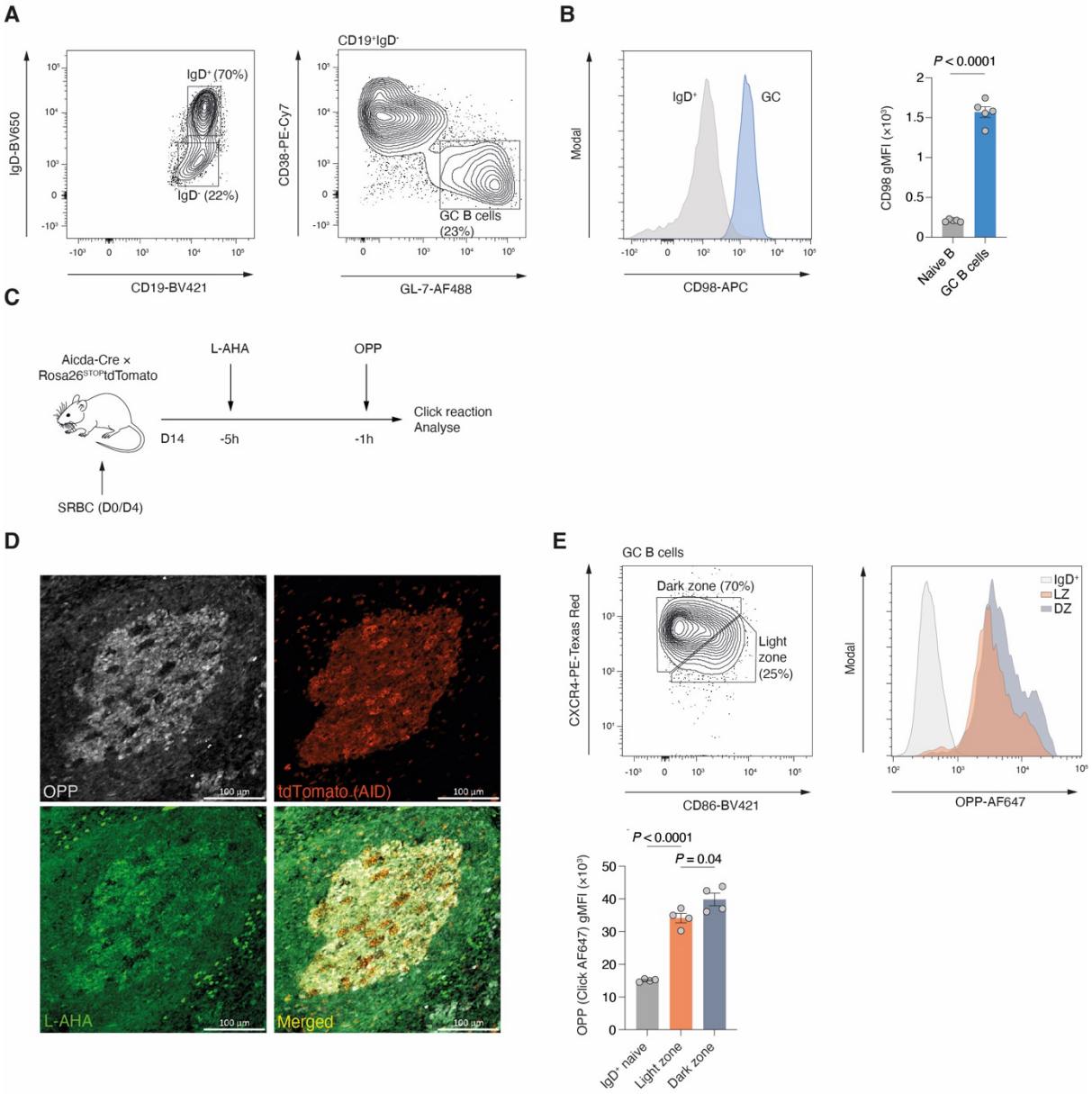

Figure 1. GC B cells have highly active protein synthesis

- **A.** Gating strategy for GC B cells ($CD19^{+}IgD^{lo}CD38^{-}GL\text{-}7^{+}$) and naïve IgD^{+} B cells ($CD19^{+}IgD^{+}$).
- **B.** Representative flow cytometry histogram and quantification of CD98 geometric mean fluorescence intensity (gMFI) in IgD^{+} naïve and GC B cells (n=5 mice). Data representative of two independent experiments.
- **C.** Schematic of in vivo bio-orthogonal non-canonical amino acid tagging. Aicda-cre × $Rosa26^{STOP}$tdTomato mice were immunised with SRBC and then boosted at day 4. At day 14, they were injected with L-AHA, and then four hours later with OPP. They were sacrificed one hour later, and non-canonical amino acid incorporation into splenic tissue was revealed using Click chemistry.

D. Representative immunofluorescence images of splenic GCs labelled with OPP, tdTomato (AID), and L-AHA. Representative of two independent experiments. Scale bar: 100µm.

E. Gating strategy, histogram, and quantification of OPP incorporation for light zone ($CD86^{hi}CXCR4^{lo}$) and dark zone ($CD86^{lo}CXCR4^{hi}$) GC B cells (n=4 mice). Representative of two independent experiments.

Statistical significance was determined by unpaired two-tailed t test (B) or one-way ANOVA with Tukey's multiple testing correction (E). Data are presented as the mean +/- SEM.

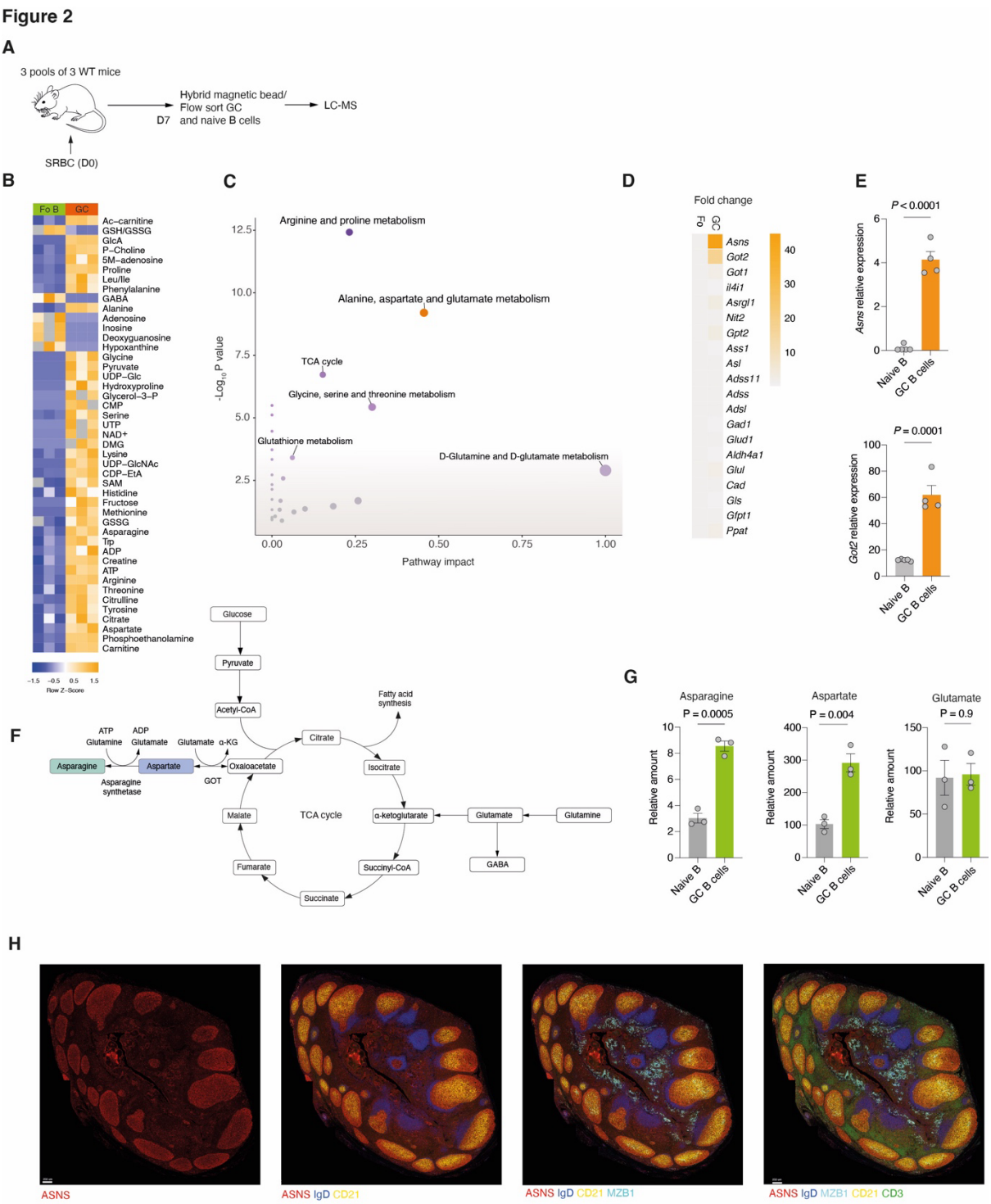

Figure 2. Asparagine metabolism is upregulated in GC B cells

- **A.** Schematic of experimental design. Three pools of three WT mice were immunised with SRBC, and at day 7 GC and follicular B cells were isolated by a hybrid magnetic bead and flow sorting approach, before analysis of polar metabolites by LC-mass spectrometry (LC-MS).
- **B.** Heatmap of significantly differentially abundant metabolites (P_{adj} <0.05) in naïve and GC B cells at day 7 from wild type mice immunised with SRBC, measured by

LC-MS (n=3 pools of 3 mice/pool). Representative of two independent experiments.

- **C.** Integrated pathway analysis of differentially abundant metabolites from **A** and expressed genes from Immgen in GC compared to naïve B cells.
- **D.** Heatmap of relative gene expression of KEGG Alanine, Aspartate, and Glutamate pathway in GC vs naïve B cells, represented as fold change. Data are from GSE133971[24].
- **E.** Relative expression of *Asns* and *Got2* in flow-sorted GC and naïve B cells from wild type mice immunised with SRBC at day 7, normalised to *Ubc* (n=4 mice). Representative of two independent experiments.
- **F.** Diagram of asparagine synthesis and its association with the TCA cycle.
- **G.** Relative amounts of asparagine, aspartate, and glutamate in GC and naïve B cells measured by LC-MS (n=3 pools of 3 mice) as in **A**. Representative of two independent experiments.
- **H.** Multiplexed Cell DIVE images of normal human tonsil section, with immunofluorescence staining for ASNS, CD21, IgD, MZB1 and CD3. Representative of 3 separate tonsils. Scale bar = 250µm.

Statistical significance was determined by two-way ANOVA with Tukey's multiple testing correction (B), hypergeometric test (C), or unpaired two-tailed t test (E, G). Data are presented as the mean +/- SEM.

Figure 3

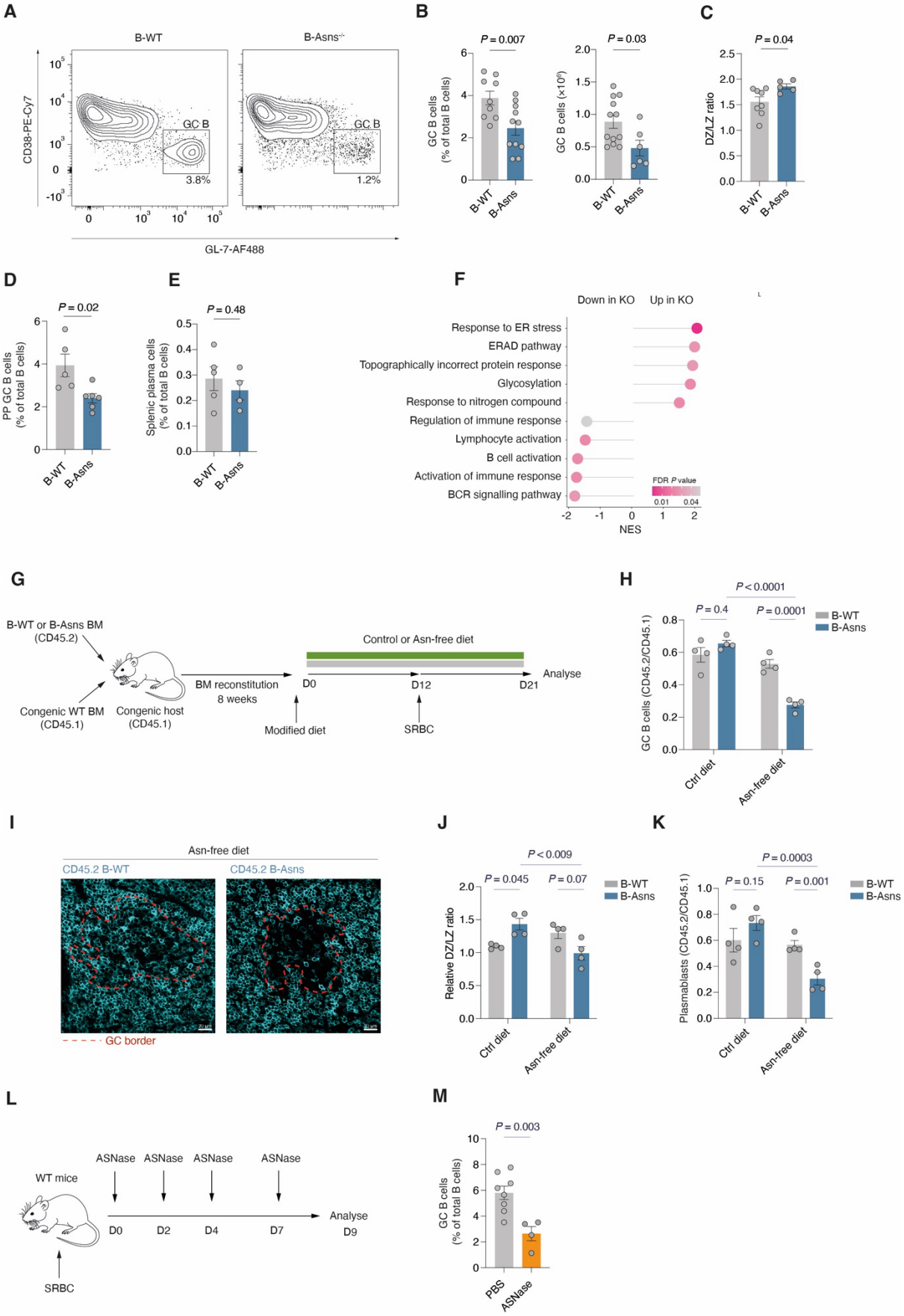
A
B-WT
B-Asns-/-
CD38-PE-Cy7
GC B
3.8%
1.2%
GL-7-AF488
B
P = 0.007
GC B cells (% of total B cells)
P = 0.03
GC B cells (×10⁶)
C
P = 0.04
DZ/LZ ratio
D
P = 0.02
PP GC B cells (% of total B cells)
E
P = 0.48
Splenic plasma cells (% of total B cells)
F
Down in KO
Up in KO
Response to ER stress
ERAD pathway
Topographically incorrect protein response
Glycosylation
Response to nitrogen compound
Regulation of immune response
Lymphocyte activation
B cell activation
Activation of immune response
BCR signalling pathway
FDR P value
0.01
0.04
NES
G
B-WT or B-Asns BM (CD45.2)
Congenic WT BM (CD45.1)
Congenic host (CD45.1)
BM reconstitution 8 weeks
Control or Asn-free diet
D0
D12
D21
Analyse
Modified diet
SRBC
H
P < 0.0001
P = 0.4
P = 0.0001
GC B cells (CD45.2/CD45.1)
Ctrl diet
Asn-free diet
I
Asn-free diet
CD45.2 B-WT
CD45.2 B-Asns
GC border
J
P < 0.009
P = 0.045
P = 0.07
Relative DZ/LZ ratio
K
P = 0.0003
P = 0.15
P = 0.001
Plasmablasts (CD45.2/CD45.1)
L
WT mice
ASNase
D0
D2
D4
D7
Analyse D9
SRBC
M
P = 0.003
GC B cells (% of total B cells)
PBS
ASNase

Figure 3. *Asns* is selectively required by GC B cells

- **A.** Representative flow cytometry plot of GC B cells ($CD19^{+}IgD^{lo}CD38^{-}GL\text{-}7^{+}$) at day 9 post-immunisation with SRBC, from B-WT and B-Asns mice.
- **B.** Quantification of proportion and number of splenic GC B cells at day 9 following SRBC immunisation (n=8 B-WT and n=11 B-Asns). Data pooled from four independent experiments.
- **C.** Ratio of DZ:LZ ($CXCR4^{hi}CD86^{lo}$:$CXCR4^{lo}CD86^{hi}$) splenic GC B cell populations (n=8 B-WT and n=5 B-Asns mice). Data pooled from two independent experiments.
- **D.** Proportion of GC B cells in Peyer's patches (n=5 B-WT and n=6 B-Asns mice). Data pooled from two independent experiments.
- **E.** Proportion of $CD138^{+}$ plasma cells in spleens of mice immunised with SRBC at day 9 (n=5 B-WT and n=4 B-Asns). Data pooled from two independent experiments.
- **F.** Gene set enrichment analysis plot of GO terms from RNA sequencing of GC B cells (n=3 B-WT and n=4 B-Asns mice) at day 9 following immunisation with SRBC.
- **G.** Schematic of BM chimera/dietary modification experiment. Mixed bone marrow chimeras were generated with B-WT or B-Asns (CD45.2) and CD45.1 wild type mice. After an 8 week reconstitution period, mice were transferred to a control (Asn-replete) or Asn-deficient diet for 12 days, before immunisation with SRBC and continuation of the diet. Mice were analysed 9 days after immunisation.
- **H.** Ratio of splenic CD45.2:CD45.1 GC B cells ($CD38^{-}BCL\text{-}6^{+}$) from bone marrow chimeric mice as described in **G**. (n=4 B-WT and n=4 B-Asns host mice). Data pooled from two independent batches.
- **I.** Representative confocal images of splenic GCs from Asn-free diet administered BM chimera hosts as described in **G**.
- **J.** Relative DZ:LZ ratio of splenic CD45.2:CD45.1 GC B cells from bone marrow chimeric mice as described in **G**. (n=4 B-WT and n=4 B-Asns donor mice). Data pooled from two independent batches.
- **K.** Ratio of splenic CD45.2:CD45.1 plasma cells ($CD138^{+}IRF4^{+}$) from bone marrow chimeric mice as described in **G**. (n=4 B-WT and n=4 B-Asns donor mice). Data pooled from two independent batches.
- **L.** Schematic of ASNase administration. Wild type mice were immunised with SRBC and injected intraperitoneally with ASNase 50U (2500U/kg) or PBS every two or three days, before analysis at day 9.
- **M.** Proportion of GC B cells from mice treated with ASNase as described in L. Representative of and pooled from two independent experiments (n=8 control and n=4 ASNase treated mice).

Statistical significance was determined by unpaired two-tailed t test (B-E, M), two-way ANOVA with Šidák's multiple testing correction multiple testing correction (H, J-K). Data are presented as the mean +/- SEM.

Figure 4

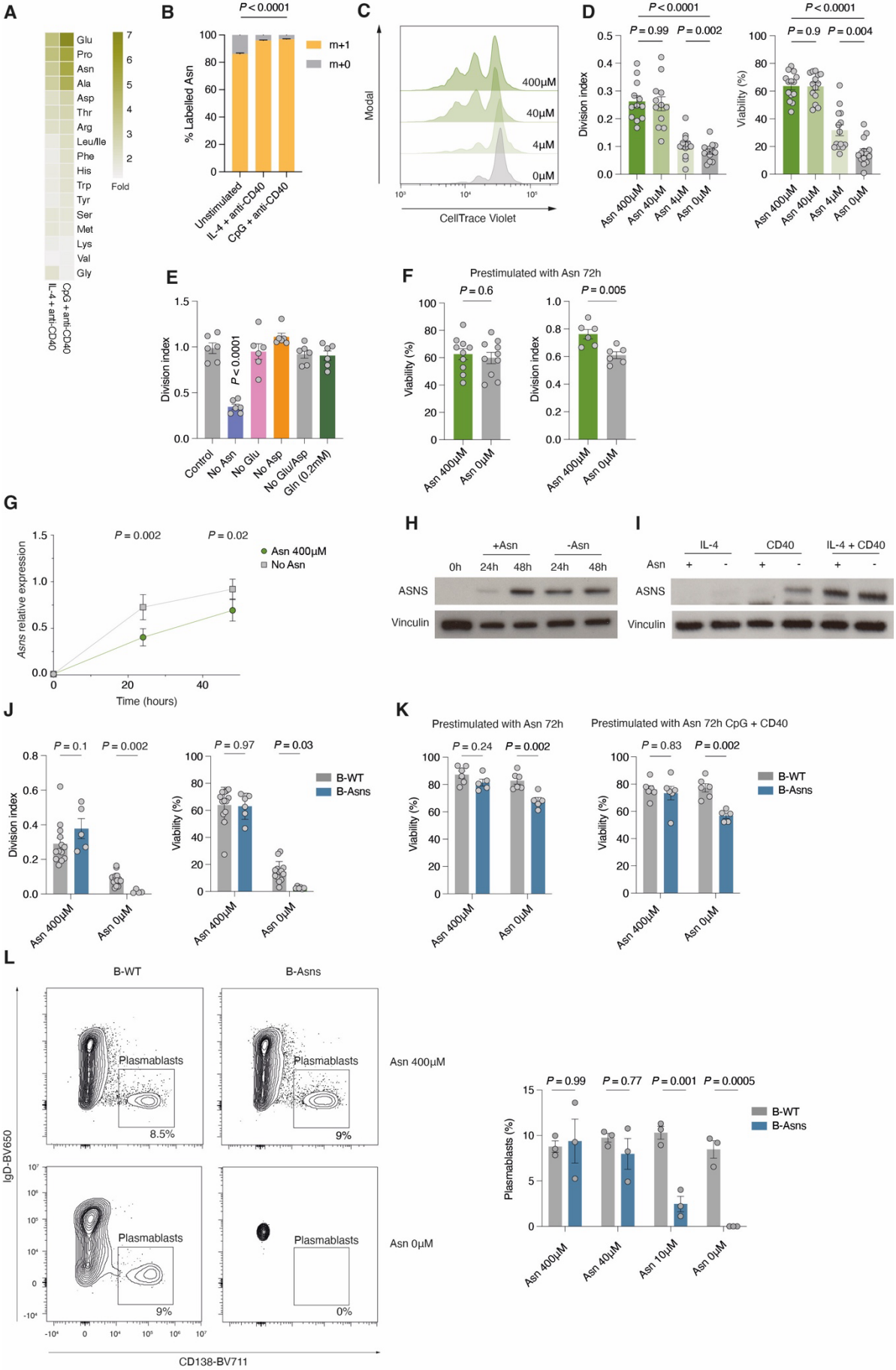
A
Glu
Pro
Asn
Ala
Asp
Thr
Arg
Leu/Ile
Phe
His
Trp
Tyr
Ser
Met
Lys
Val
Gly
IL-4 + anti-CD40
CpG + anti-CD40
Fold
B
P < 0.0001
% Labelled Asn
m+1
m+0
Unstimulated
IL-4 + anti-CD40
CpG + anti-CD40
C
Modal
400μM
40μM
4μM
0μM
CellTrace Violet
D
P < 0.0001
P = 0.99
P = 0.002
Division index
Viability (%)
P = 0.9
P = 0.004
Asn 400μM
Asn 40μM
Asn 4μM
Asn 0μM
E
Division index
P < 0.0001
Control
No Asn
No Glu
No Asp
No Glu/Asp
Gln (0.2mM)
F
Prestimulated with Asn 72h
P = 0.6
P = 0.005
Viability (%)
Division index
Asn 400μM
Asn 0μM
G
P = 0.002
P = 0.02
Asn 400μM
No Asn
Asns relative expression
Time (hours)
H
+Asn
-Asn
0h
24h
48h
24h
48h
ASNS
Vinculin
I
IL-4
CD40
IL-4 + CD40
Asn
+
-
+
-
+
-
ASNS
Vinculin
J
P = 0.1
P = 0.002
P = 0.97
P = 0.03
Division index
Viability (%)
B-WT
B-Asns
Asn 400μM
Asn 0μM
K
Prestimulated with Asn 72h
Prestimulated with Asn 72h CpG + CD40
P = 0.24
P = 0.002
P = 0.83
P = 0.002
Viability (%)
B-WT
B-Asns
Asn 400μM
Asn 0μM
L
B-WT
B-Asns
Plasmablasts
8.5%
9%
Asn 400μM
9%
0%
Asn 0μM
IgD-BV650
CD138-BV711
P = 0.99
P = 0.77
P = 0.001
P = 0.0005
Plasmablasts (%)
B-WT
B-Asns
Asn 400μM
Asn 40μM
Asn 10μM
Asn 0μM

Figure 4. Asn controls B cell homeostasis

- **A.** Heatmap of fold change of indicated amino acids in B cells, measured by LC-MS following stimulation for 24h with IL-4 and anti-CD40, or CpG and anti-CD40, relative to unstimulated condition (n=3 mice). Representative of two independent experiments.
- **B.** Fraction of labelling of intracellular Asn with ^{15}N in B cells stimulated as in **A**, in the presence of $^{15}N_1$-Asn (n=3 mice). Representative of two independent experiments.
- **C.** Representative histogram of dilution of Celltrace Violet in B cells stimulated with IL-4 and anti-CD40 and cultured for 72h with the indicated concentration of Asn.
- **D.** Viability and division index of B cells stimulated with IL-4 and anti-CD40 and cultured for 72h with the indicated concentration of Asn (n=10 mice). Representative of and pooled from three independent experiments.
- **E.** Division index of B cells stimulated for 72h with IL-4 and anti-CD40 in the presence or absence of the indicated amino acids (n=6 mice). Representative of and pooled from three independent experiments.
- **F.** Viability and division index of B cells stimulated with IL-4 and anti-CD40 with 400µM Asn for 72h, then restimulated for an additional 24h in the presence or absence of Asn (n=6-10 mice). Representative of and pooled from two independent experiments.
- **G.** Quantification of relative expression of *Asns* at the indicated timepoints in B cells stimulated with IL-4 and anti-CD40 in the presence or absence of Asn (n=3 mice). Representative of two independent experiments.
- **H.** Representative immunoblot of ASNS in B cells stimulated with IL-4 and anti-CD40 with or without Asn, at the indicated timepoints. Representative of two independent experiments.
- **I.** Representative immunoblot of ASNS in B cells stimulated for 48h with IL-4, anti-CD40, or IL-4 and anti-CD40, with or without Asn. Representative of two independent experiments.
- **J.** Viability and division index of B cells from B-Asns and B-WT mice stimulated for 72h with IL-4 and anti-CD40 in the presence or absence of Asn (n=13 B-WT and n=5-6 B-Asns mice). Representative of and pooled from >4 independent experiments.
- **K.** Viability and division index of B cells from B-Asns and B-WT mice stimulated with IL-4 and anti-CD40 or CpG and anti-CD40, with Asn for 72h, then restimulated for an additional 24h in the presence or absence of Asn (n=6 B-WT and n=5-6 B-Asns mice). Representative of and pooled from two independent experiments.
- **L.** Representative flow cytometry plots and quantification of $IgD^{-}CD138^{+}$ Plasmablast proportions in B cells from B-WT and B-Asns mice stimulated with LPS and IL-4 for 72h at the indicated concentration of Asn. Representative of three independent experiments.

Statistical significance was determined by one-way ANOVA with Tukey's multiple testing correction (B,D-E, G), unpaired two-tailed t test (F), or two-way ANOVA with Šidák's multiple testing correction (G,J-L). Data are presented as the mean +/- SEM.

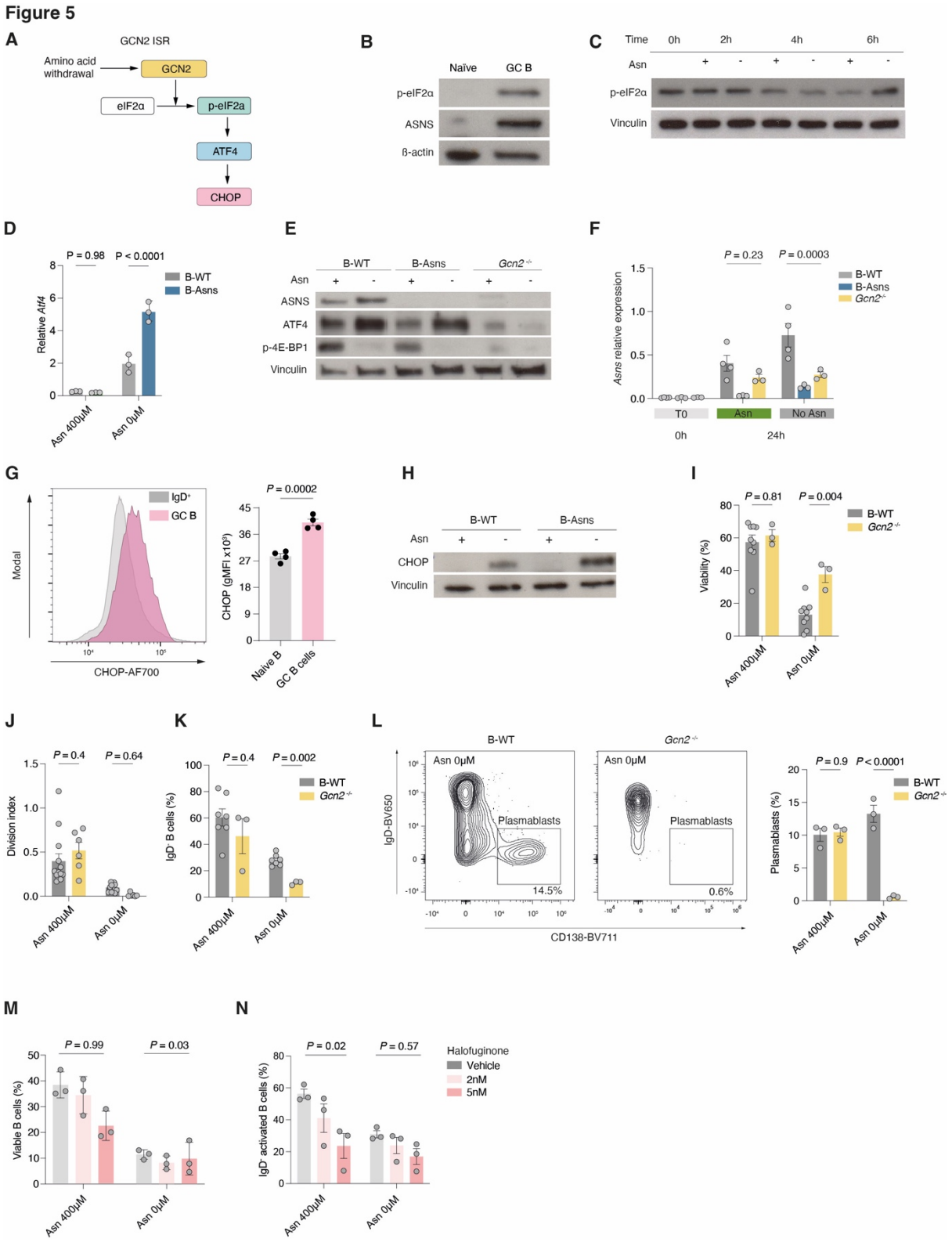

Figure 5. The integrated stress response regulates B cell function through ASNS

- **A.** Schematic of the GCN2 branch of the integrated stress response.
- **B.** Immunoblot of phospho-eIF2α and ASNS in magnetic bead sorted GC B cells and naïve B cells, from wild type mice immunised with SRBC at D0 and D4, with analysis

at D12. Representative of two independent experiments. Beta-actin is used as a loading control.

- **C.** Representative immunoblot time course of phospho-eIF2α in wild type B cells stimulated with IL-4 and agonistic anti-CD40 in the presence or absence of Asn (400µM). Representative of two independent experiments.
- **D.** Relative expression of *Atf4* in B-Asns and B-WT B cells stimulated for 72h in the presence or absence of Asn (n=3 B-WT and n=3 B-Asns mice). Representative of two independent experiments.
- **E.** Representative immunoblot of ASNS, ATF4, phospho-eIF2α in B cells from B-Asns, *Gcn2*$^{-/-}$, and B-WT mice, stimulated for 24h with anti-CD40 and IL-4 in the presence or absence of Asn (400µM). Representative of two independent experiments. Vinculin used as loading control.
- **F.** Relative expression of *Asns* by qPCR in freshly isolated (T=0) and stimulated (IL-4 and anti-CD40 for 24h) B cells (n=4 B-WT, n=3 B-Asns, and n=3 *Gcn2*$^{-/-}$ mice). Representative of two independent experiments.
- **G.** Representative flow cytometry histogram of CHOP intracellular staining in GC B cells and IgD^{+} naïve B cells at D9 following immunisation with SRBC, with quantification of geometric mean fluorescence intensity (n=3 wild type mice). Representative of two independent experiments.
- **H.** Representative immunoblot of CHOP in B-WT or B-Asns B cells stimulated with IL-4 and anti-CD40 for 24h, in the presence or absence of Asn (400µM). Representative of two independent experiments. Vinculin used as loading control.
- **I.** Viability of *Gcn2*$^{-/-}$ and wild type B cells stimulated with IL-4 and agonistic anti-CD40 for 72h, in the presence or absence of Asn (400µM)(n=3 *Gcn2*$^{-/-}$ mice and n=9 wild type mice). Representative of and pooled from three independent experiments.
- **J.** Division index of *Gcn2*$^{-/-}$ and wild type B cells stimulated with IL-4 and agonistic anti-CD40 for 72h, in the presence or absence of Asn (400µM)(n=6 *Gcn2*$^{-/-}$ mice and n=13 wild type mice). Representative of and pooled from four independent experiments.
- **K.** Flow cytometry quantification of IgD expression in *Gcn2*$^{-/-}$ and wild type B cells as in **I**. Representative of and pooled from two independent experiments.
- **L.** Representative flow cytometry gating and quantification of plasmablast (IgD^{-} CD138^{+}) differentiation of *Gcn2*$^{-/-}$ and wild type B cells following stimulation with LPS (10µg/ml) and IL-4 (50ng/ml) for 72h in the presence or absence of Asn (400µM) (n=3 *Gcn2*$^{-/-}$ mice and n=3 wild type mice). Data pooled from two independent experiments.
- **M.** Viability of wild type B cells stimulated with IL-4 and agonistic anti-CD40 for 72h, in the presence or absence of Asn (400µM), and with the indicated concentration of halofuginone or vehicle. Representative of two independent experiments.
- **N.** Flow cytometry quantification of IgD expression as in **M**. Representative of two independent experiments.

Statistical significance was determined by unpaired two-tailed t test (G) or two-way ANOVA with Šidák's multiple testing correction (D,F,I-N). Data are presented as the mean +/- SEM.

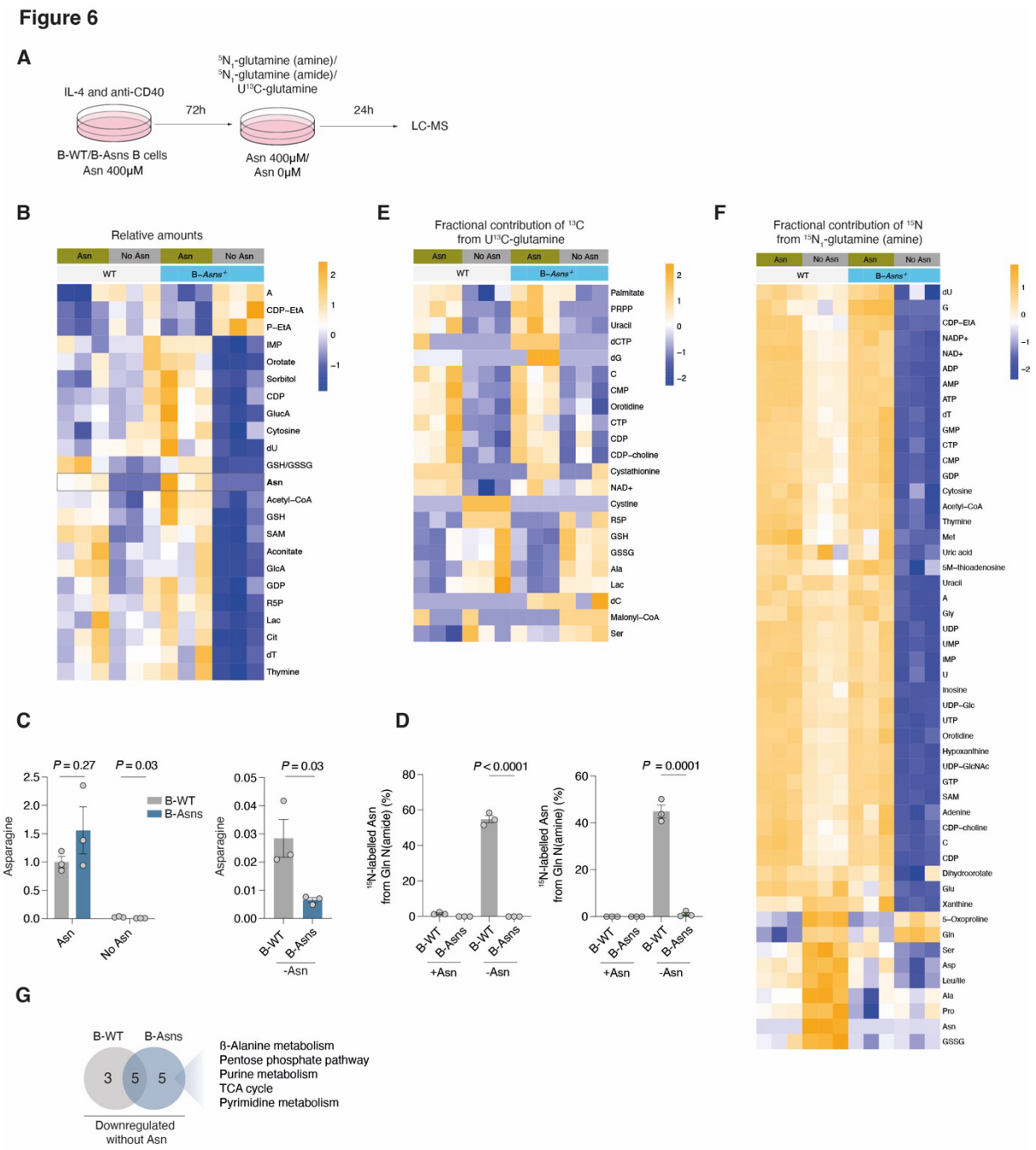

Figure 6. Disruption of asparagine availability alters B cell metabolism

- **A.** Schematic of experimental design for stable isotope-resolved metabolomics. B-WT or B-Asns B cells were stimulated with IL-4 and agonistic anti-CD40 for 72 hours in the presence of Asn (400µM), then stimulated for an additional 24h with or without Asn (400µM), and either $^{15}N_1$(amine)-glutamine, $^{15}N_1$(amide)-glutamine, U^{13}C-glutamine, or unlabelled glutamine, before analysis by LC-MS.
- **B.** Heatmap of total relative amounts of significantly different metabolites in B cells from B-WT or B-Asns mice as in **A**. Scale represents row Z-score. Significantly differentially abundant metabolites ($P_{adj} < 0.05$) are shown. Representative of two independent experiments.

C. Abundance of intracellular Asn in B cells cultured as in **A**, and rescaled plot of Asn-deprived condition. Representative of two independent experiments.

D. Fractional contribution of ^{15}N to Asn pool, derived from $^{15}N_1$-amino or amide Gln, following culture as described in **A**.

E. Heatmap of fractional contribution of ^{13}C to indicated metabolites, derived from U-^{13}C-Gln following culture as described in **A**. Scale represents row Z-score. Significantly differentially labelled metabolites ($P_{adj} < 0.05$) are shown.

F. Heatmap of fractional contribution of ^{15}N to indicated metabolites, derived from $^{15}N_1$-amine Gln following culture as described in **A**, with labelled compound added for final 24h of culture. Scale represents row Z-score. Significantly differentially labelled metabolites ($P_{adj} < 0.05$) are shown.

G. Venn-diagram indicating number of significantly differentially-regulated pathways in B-WT and B-Asns B cells following Asn-withdrawal, based on relative metabolite abundance as in **B**. Listed pathways are those specifically downregulated in B-Asns B cells.

Statistical significance was determined by two-way ANOVA with Šidák's multiple testing correction (B, C, D-F), hypergeometric test (G) or unpaired two-tailed t test (C). Data are presented as the mean +/- SEM.

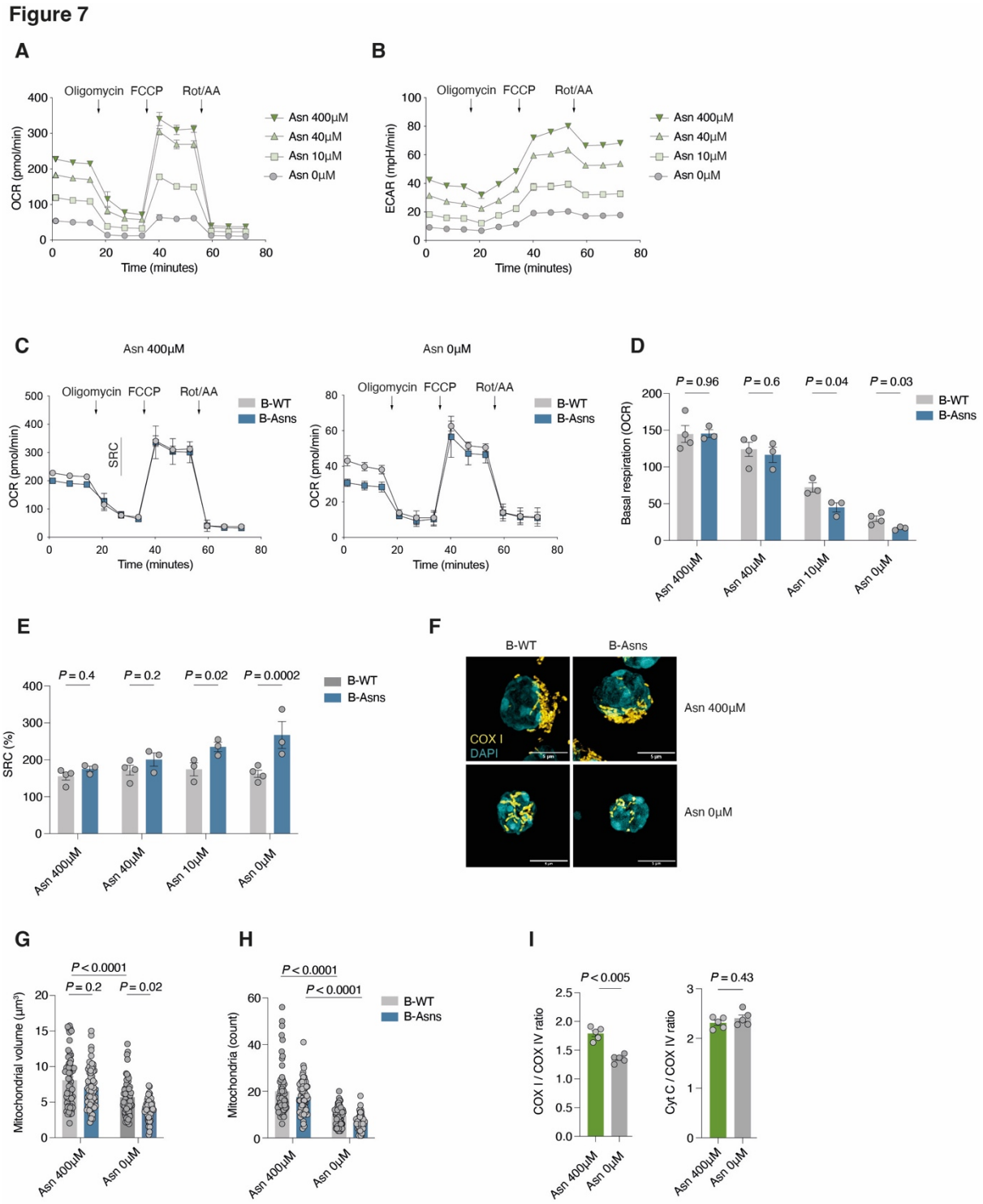

Figure 7. Mitochondrial function in B cells requires Asn

- **A.** Seahorse extracellular flux analysis of B cells stimulated for 24h with IL-4 and agonistic anti-CD40 at the indicated concentrations of Asn. Oxygen consumption rate (OCR) was measured during the MitoStress test. Representative of three independent experiments with 5-6 technical replicates.
- **B.** Seahorse extracellular flux analysis of B cells as in **A**. Extracellular acidification rate (ECAR) was measured during the MitoStress test. Representative of three independent experiments with 5-6 technical replicates.

C. Seahorse extracellular flux analysis of OCR in B-WT (n=4 mice) and B-Asns (n=3 mice) B cells stimulated for 24h with IL-4 and agonistic anti-CD40 at the indicated concentrations of Asn. Spare respiratory capacity (SRC) is illustrated. Representative of three independent experiments.

D. Quantification of basal OCR in B-WT and B-Asns B cells stimulated for 24h with IL-4 and agonistic anti-CD40 at the indicated concentrations of Asn. Representative of three independent experiments.

E. Quantification of SRC (%) as in **D**.

F. 3D Lattice SIM images of COX I and DAPI in B-WT and B-Asns B cells (pooled from n=3 mice) stimulated for 24h with IL-4 and agonistic anti-CD40 in the presence or absence of Asn (400µM). Representative of three independent experiments.

G. Quantification of mitochondrial volume as in **F**.

H. Quantification of mitochondrial count as in **F**.

I. Quantification of gMFI of ETC subunits COX I and CytC relative to COX IV by flow cytometry in wild type B cells (n=5 mice) stimulated for 24h with IL-4 and agonistic anti-CD40 in the presence or absence of Asn (400µM). Pooled from three independent experiments after batch correction.

Statistical significance was determined by two-way ANOVA with Šidák's multiple testing correction (D-E, G-H), or unpaired two-tailed t test after batch correction (I). Data are presented as the mean +/- SEM.

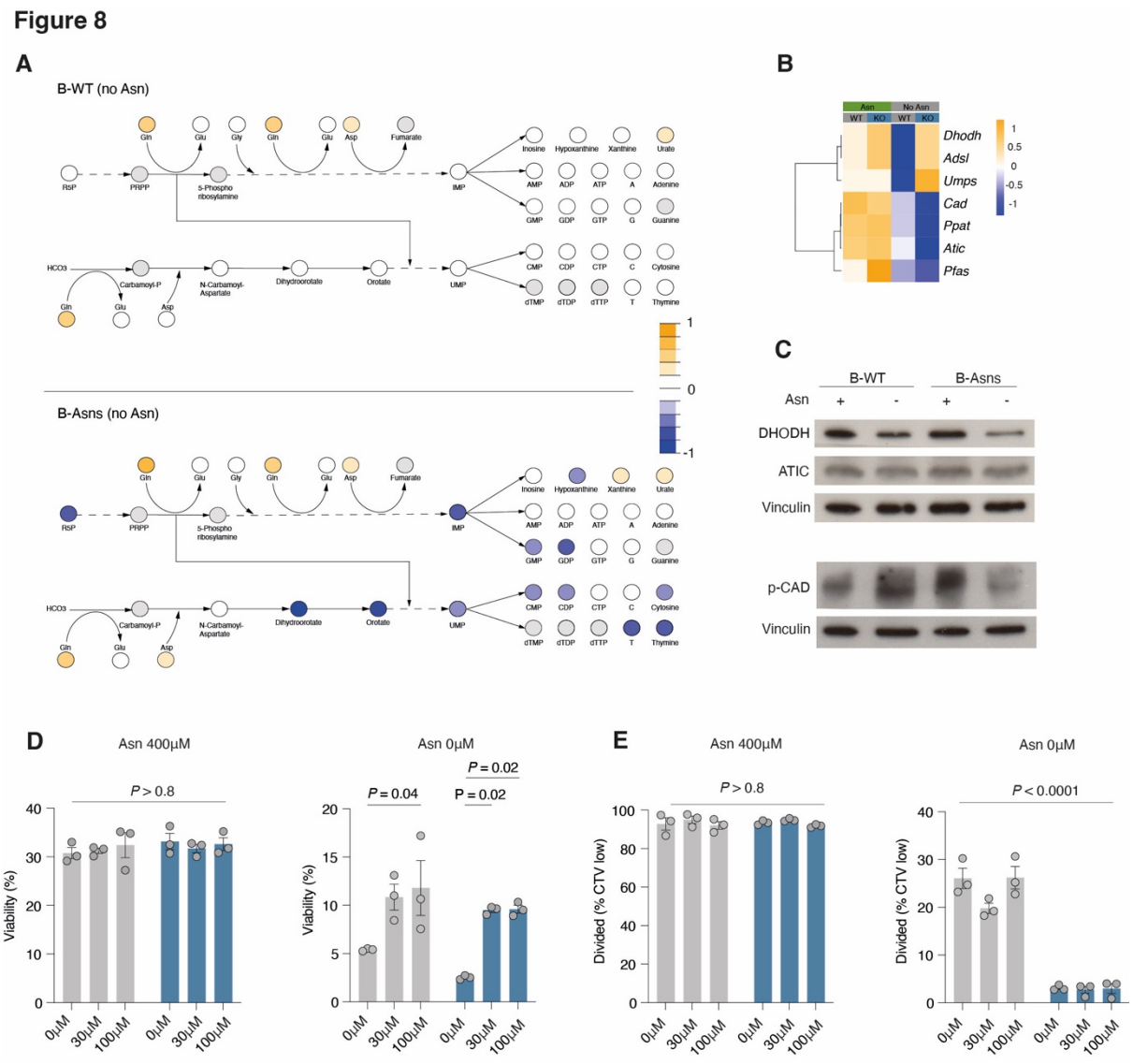

Figure 8. ASNS gates nucleotide synthesis in B cells

- **A.** Relative abundance of metabolites in nucleotide synthesis pathway in B-WT and B-Asns B cells deprived of Asn. Grey-filled circles indicate that the metabolite was not detected. Scale represents abundance ratio.
- **B.** Heatmap of relative expression of indicated genes in B cells from B-Asns and B-WT mice cultured for 72h with IL-4 and anti-CD40 and quantified by RT-qPCR. Each heatmap cell represents the mean of 3 individual mice (B-WT and B-Asns). Representative of two independent experiments.
- **C.** Representative immunoblot of DHODH, ATIC, phospho-CAD in B-WT or B-Asns B cells stimulated with IL-4 and anti-CD40 for 24h, in the presence or absence of Asn (400µM). Representative of two independent experiments. Vinculin used as loading control.
- **D.** Viability of B cells from B-Asns and B-WT mice (n=3 mice) stimulated for 72h with IL-4 and anti-CD40 in the presence or absence of Asn supplemented with adenosine, thymidine, uridine, cytidine, and guanosine at 0µM, 30µM or 100µM. Data pooled from two independent experiments.

E. Quantification of the fraction of B cells from B-Asns and B-WT mice (n=3 mice) having diluting Celltrace Violet after stimulation for 72h with IL-4 and anti-CD40 in the presence or absence of Asn supplemented with adenosine, thymidine, uridine, cytidine, and guanosine at 0µM, 30µM or 100µM. Data pooled from two independent experiments.

Statistical significance was determined by two-way ANOVA with Šidák's multiple testing correction (D,E). Data are presented as the mean +/- SEM.

Extended Data Figure 1

A

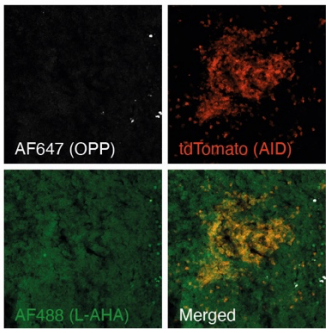

Extended Data Figure 1.

A. Representative immunofluorescence images of splenic GCs labelled with PBS as a negative control for **Fig 1D.** Representative of two independent experiments.

Extended Data Figure 2

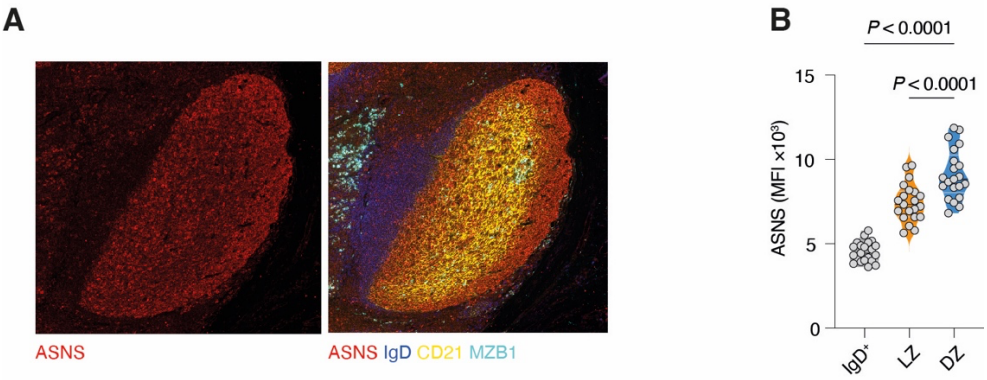

Extended Data Figure 2.

- **A.** Cell DIVE ASNS immunofluorescence images of a GC from a tonsil highlighting CD21^{+} LZ, CD21^{-} DZ, IgD^{+} naïve, and MZB1^{+} plasma cell niches.
- **B.** Quantification of mean fluorescence intensity (MFI) of ASNS in areas shown in **A**. Each dot represents a randomly-selected GC with a DZ, LZ and surrounding IgD^{+} naïve B cell follicle (n=21 GCs in total, pooled from three tonsils).

Statistical significance was determined by one-way ANOVA with Tukey's multiple testing correction (B). Data are presented as the mean +/- SEM.

Extended Data Figure 3

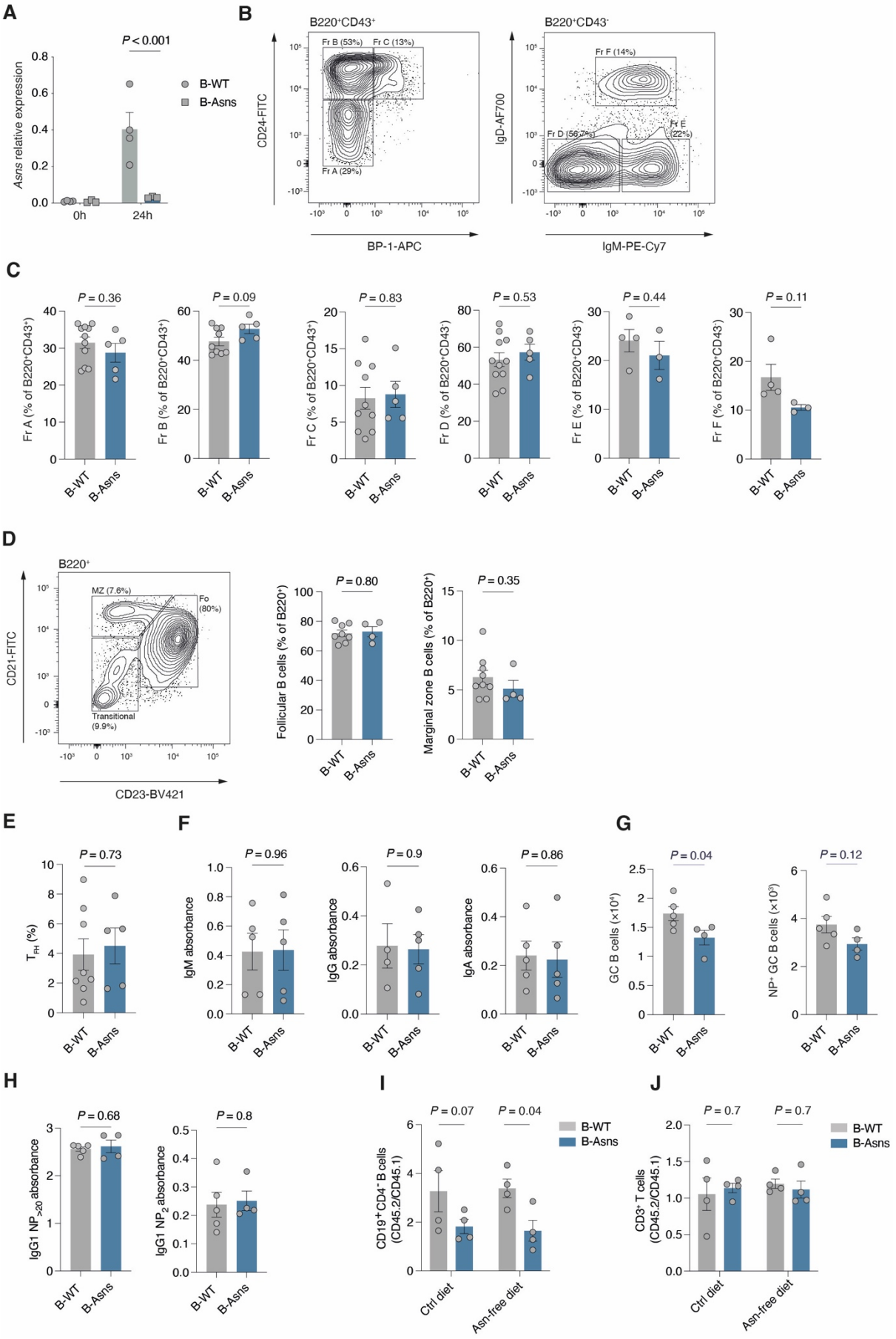

Extended Data Figure 3.

- **A.** Relative expression of *Asns* by qPCR in freshly isolated, and stimulated (IL-4 and anti-CD40 for 24h) B cells (n=4 B-WT and n=4 B-Asns mice). Representative of two independent experiments.
- **B.** Representative gating strategy for indicated Hardy stages of B cell development in bone marrow.
- **C.** Quantification of indicated Hardy stages of B cell development in bone marrow (n=11 B-WT and n=5 B-Asns mice). Data pooled from two independent experiments.
- **D.** Representative gating strategy for transitional, marginal zone, and follicular B cells in spleen and quantification (n=8 B-WT and n=4 B-Asns). Data pooled from two independent experiments.
- **E.** Quantification of CXCR5^{+} PD-1^{hi} T_{FH} in CD4^{+} T cell compartment (n=8 B-WT and n=5 B-Asns) at D9 following SRBC immunisation. Data pooled from two independent experiments.
- **F.** ELISA quantification of IgM, IgG and IgA levels at steady state in unimmunised B-WT and B-Asns (n=5 mice). Data representative of two independent experiments.
- **G.** Quantification of total and NP-binding GC B cell counts in B-WT and B-Asns inguinal lymph nodes at D14 following subcutaneous NP-CGG immunisation. Data representative of three independent experiments.
- **H.** High affinity (NP_2) and low affinity ($NP_{>20}$) NP-specific IgG1 levels from B-WT and B-Asns mice immunised as in **G**.
- **I.** Relative reconstitution of total peripheral CD19^{+} B cell compartment in 50:50 competitive bone marrow chimera (as in Fig. **3G**).
- **J.** Relative reconstitution of total peripheral CD3^{+} T cell compartment in 50:50 competitive bone marrow chimera (as in Fig. **3G**).

Statistical significance was determined by unpaired two-tailed t test (C-H), or two-way ANOVA with Šidák's multiple testing correction (A,I,J) . Data are presented as the mean +/- SEM.

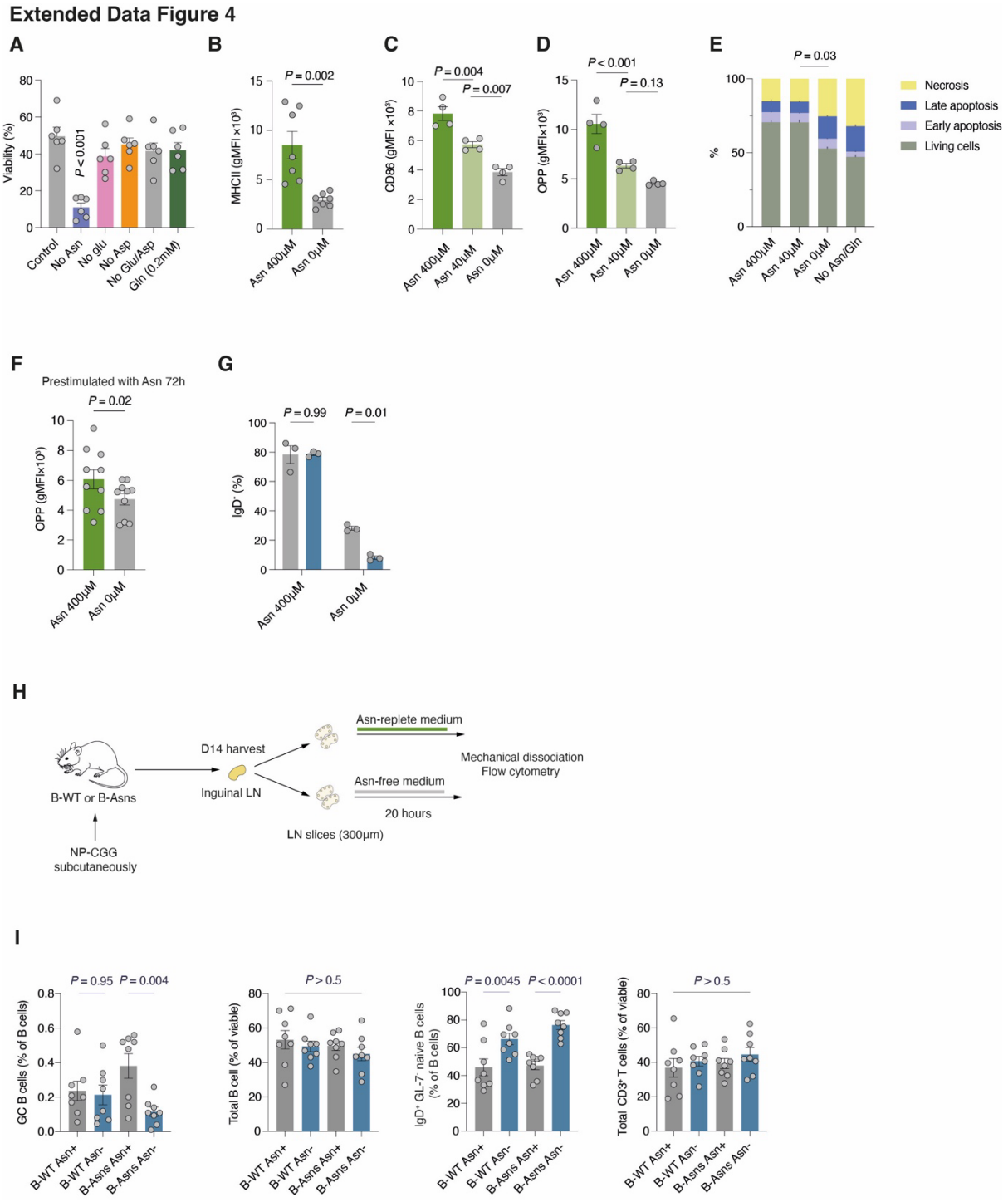

Extended Data Figure 4.

A. Viability of B cells stimulated for 72h with IL-4 and anti-CD40, in the presence or absence of the indicated amino acids (n=6 mice). Representative of three independent experiments.

B. MHCII gMFI in B cells stimulated for 24h with IL-4 and anti-CD40 with the indicated concentrations of Asn (n=7 mice). Representative of and pooled from three independent experiments.

C. CD86 gMFI in B cells stimulated for 24h with IL-4 and anti-CD40 with the indicated concentrations of Asn (n=4 mice). Representative of three independent experiments.

D. OPP incorporation determined by flow cytometry in B cells stimulated for 24h with IL-4 and anti-CD40 with the indicated concentrations of Asn (n=4 mice). Representative of two independent experiments.

E. Quantification of stages of apoptosis in B cells stimulated with IL-4 and anti-CD40 at 18h, defined by annexin V labelling and propidium iodide staining, in the presence/absence of Asn or Asn and Gln (n=3 individual mice). Representative of two independent experiments.

F. OPP incorporation of B cells stimulated for 72h with IL-4 and anti-CD40 in the presence Asn, then restimulated for an additional 24h in the absence of Asn (n=10 mice). Representative of and pooled from two independent experiments.

G. Quantification of IgD^- activated B cells by flow cytometry following stimulation with IL-4 and anti-CD40 in the presence or absence of Asn (400µM) for 72h from B-WT and B-Asns mice (n=3 mice). Representative of three independent experiments.

H. Schematic of lymph node slice culture system. B-WT and B-Asns mice were immunised with NP-CGG subcutaneously and inguinal lymph nodes were harvested at D14. 300µm thick slices were cultured for 20h in the presence or absence of Asn in duplicates and analysed by flow cytometry.

I. Quantification of $CD38^-GL\text{-}7^+$ GC B, $CD19^+$ $CD3^-$ total B, $IgD^+GL\text{-}7^-$ naïve B, and $CD3^+$ T cell proportions by flow cytometry in lymph node slices cultured for 20h in the presence or absence of Asn (400µM). Each dot represents single lymph node (n=8 lymph nodes from n=4 mice).

Statistical significance was determined by one-way ANOVA with Tukey's multiple testing correction (A,C-E), unpaired two-tailed t test (B, F), or two-way ANOVA with Šidák's multiple testing correction (G,I). Data are presented as the mean +/- SEM.

Extended Data Figure 5

A

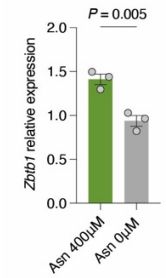

Extended Data Figure 5.

A. Relative expression of *Zbtb1* by qPCR in B cells stimulated with IL-4 and anti-CD40 from wild type mice (n=3), in the presence or absence of Asn. Representative of two independent experiments.

Statistical significance was determined by unpaired two-tailed t test. Data are presented as the mean +/- SEM.

Extended Data Figure 6

A

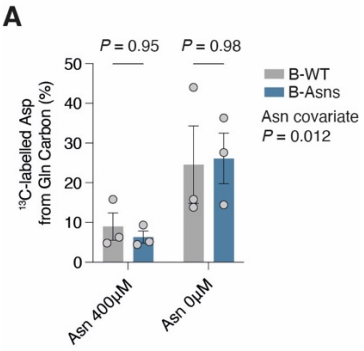

Extended Data Figure 6.

- **A.** Percentage of aspartate labelled with ^{13}C, indicating derivation from U^{13}C-glutamine, as in Fig. **6E**.

Statistical significance was determined by two-way ANOVA with Šidák's multiple testing correction, with Asn concentration as a co-variate. Data are presented as the mean +/- SEM.

Extended Data Figure 7

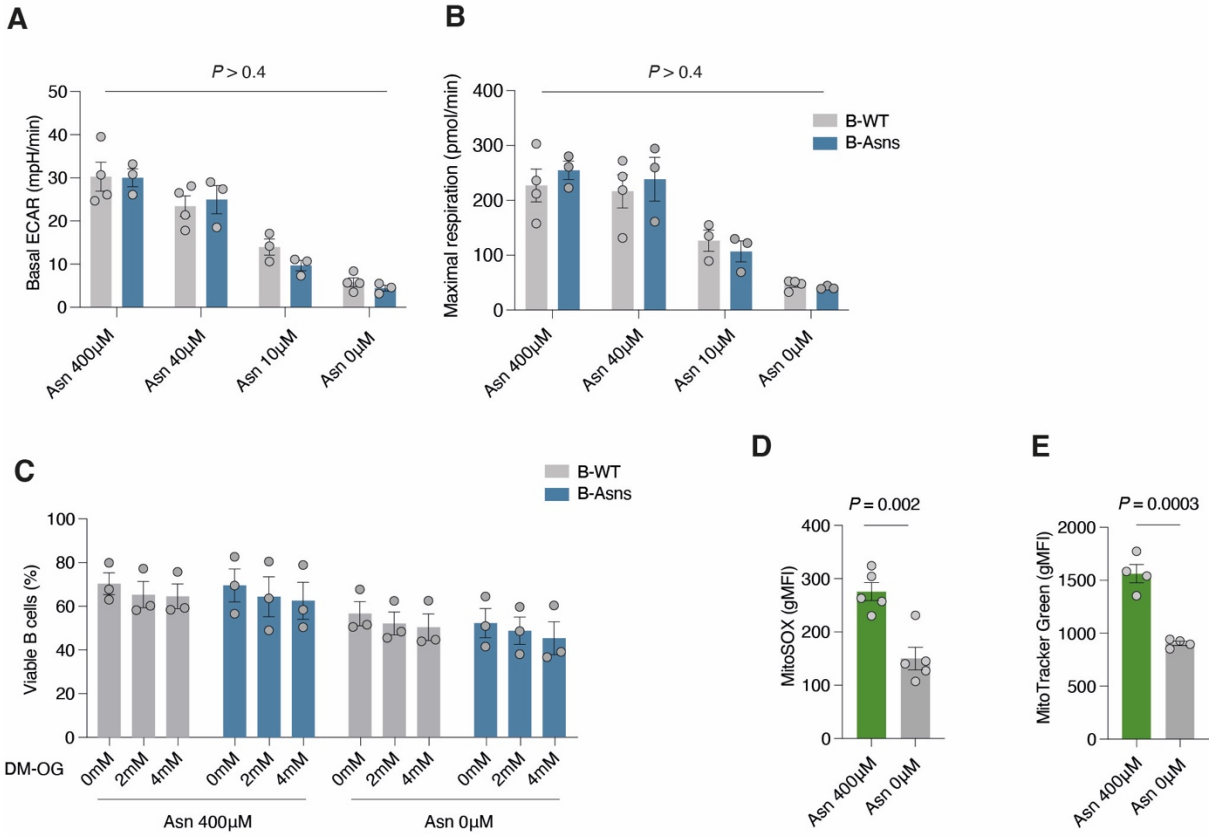

Extended Data Figure 7.

A. Quantification of ECAR as in Fig. 7B.
B. Quantification of maximal respiration as in Fig. 7D.
C. Viability of B cells from B-WT and B-Asns stimulated with anti-CD40 and IL-4 for 24h in the presence or absence of Asn (400µM), supplemented with vehicle or DM-OG at the indicated concentrations (0mM, 2mM and 4mM). Data pooled from two independent experiments (n=3 B-WT, n=3 B-Asns mice).
D. MitoSOX gMFI of wild type B cells stimulated for 18h with IL-4 and anti-CD40, in the presence or absence of Asn (n=5 mice). Representative of two independent experiments.
E. MitoTracker Green gMFI of wild type B cells stimulated for 18h with IL-4 and anti-CD40, in the presence or absence of Asn (n=4 mice). Representative of two independent experiments.

Statistical significance was determined by two-way ANOVA with Šidák's multiple testing correction (A-B), one way ANOVA with Tukey's multiple testing correction (C) or unpaired two-tailed t test (D-E). Data are presented as the mean +/- SEM.

Material and methods

Mice

C57BL/6J mice were obtained from Envigo. C57BL/6N-*Asns*$^{tm1c(EUCOMM)Wtsi}$/H (EM:05307) mice were obtained from the Mary Lyon Centre, MRC Harwell, UK. B6.129S6-*Eif2ak4*$^{tm1.2Dron}$/J (JAX: 008240), B6.C(Cg)-*Cd79a*$^{tm1(cre)Reth}$/EhobJ (JAX: 020505), B6.129P2-*Aicda*$^{tm1(Cre)Mnz}$/J (JAX: 007770), and B6;129S6-*Gt(ROSA)26Sor*$^{tm9(CAG-tdTomato)Hze}$/J (JAX: 007905) mice were obtained from Jackson Laboratories. B6.SJL.CD45.1 mice were provided by the central breeding facility of the University of Oxford. Male and female mice between the ages of 6-15 weeks were used. Mice were bred and maintained under specific pathogen-free conditions at the Kennedy Institute of Rheumatology, University of Oxford. They were housed in cages that had individual ventilation and were provided with environmental enrichment. The temperature was kept between 20-24°C, with a humidity level of 45-65%. They were exposed to a 12-hour cycle of light and darkness (7 am to 7 pm), with a thirty-minute period of dawn and dusk. All procedures and experiments were performed in accordance with the UK Scientific Procedures Act (1986) under a project license authorized by the UK Home Office (PPL number: PP1971784).

Bone marrow chimera generation

B6.SJL.CD45.1 recipient mice were administered two doses of 5.5Gy irradiation four hours apart. Mice were then intravenously injected with 4×10^6 mixed bone marrow (BM) cells at a 1:1 ratio, isolated from age- and sex-matched CD45.2$^+$ B-WT or B-Asns and CD45.1$^+$ WT donor mice. Recipient mice were maintained on antibiotics (Baytril, Bayer corporation) administered in their drinking water for two weeks. Bone marrow reconstitution was confirmed by flow cytometry of peripheral blood at 8 weeks. Asn-free diet or control chow (Research Diets, A05080216i and A10021Bi) was administered for 12 days starting from week 8, maintained for additional 9 days (total of 21 days) during immunisation with SRBC until mice were terminated at 11 weeks.

Immunisation

1ml of sterile SRBCs in Alsever's solution (ThermoFisher or EO Labs) were washed twice with 10ml of ice-cold PBS and reconstituted in 3ml of PBS, and 200µl injected intraperitoneally or intravenously. In some experiments, an enhanced SRBC immunisation method was used to maximise GC B cell yield by immunising mice with 0.1ml SRBC on day 0 followed by a second injection of 0.2ml on day 5[46]. For protein antigen immunisations, 50µg $NP_{(30-39)}$-CGG (Biosearch Tech, cat: N-5055D-5) in PBS was mixed with Imject Alum (ThermoFisher) or Alum Hydrogel (InvivoGen, cat: vac-alu-50) at a 1:1 ratio (vol:vol) and rotated at room temperature for 30 mins before intraperitoneal injection in 100µl volume, or mixed vigorously with a pipette for 5 mins before subcutaneous injection on the flanks.

Asparaginase treatment

Wild type mice were immunised with SRBC, and 50U (2500U/kg) of asparaginase diluted in PBS from *E. coli* (Abcam) was administered by intraperitoneal injection at days 0,2,4, and 7 total of four doses. Spleens were collected at day 9 for analysis by flow cytometry.

Cell isolation

Spleens were dissociated by passing through 70µm cell strainers. For ex vivo GC B cell mass spectrometry, GC B cells were first enriched using the mouse Germinal Center B Cell (PNA) MicroBead Kit (Miltenyi), and then purified by flow sorting (Live/Dead$^-$CD19$^+$IgD$^-$GL-7$^+$CD95$^+$). Total B cells from the same mouse pool were pre-enriched using CD19$^+$ Microbeads (Miltenyi), then naïve B cells purified by flow sorting (Live/Dead$^-$B220$^+$IgD$^+$). To isolate cells for RNA extraction, GC B cells (Live/Dead$^-$CD19$^+$IgD$^-$CD95$^+$GL-7$^+$) and naïve B cells (Live/Dead$^-$CD19$^+$IgD$^+$) were flow sorted into RLT Plus buffer (Qiagen) following pre-enrichment with the Pan B Cell Isolation Kit II (Miltenyi). B cells for culture were isolated using the Pan B Cell Isolation Kit II (Miltenyi). Purity was routinely >90% by flow cytometry.

For some experiments, untouched GC B cells were isolated using a magnetic bead-based protocol as described[47]. Briefly, single cell suspensions were prepared from spleens of SRBC-immunised mice (enhanced protocol) in ice cold MACS isolation buffer (PBS with 0.5% BSA and 2mM EDTA) followed by ACK (Gibco) RBC lysis for 4 mins at 20°C. Following washing, cells were labelled with anti-CD43 microbeads (Miltenyi) and biotinylated antibodies against CD38 and CD11c (both eBioscience, clones 90 and N418 respectively). Then, cells were incubated with Microbeads (Miltenyi), and subsequently run through an LS column (Miltenyi). GC B cell purity was around 95%.

Cell culture

Total B cells were isolated as described above. B cells were cultured at 1-3×10^6 cells/ml in RPMI1640 (custom product from Cell Culture Technologies, Gravesano, Switzerland, lacking glutamate, aspartate, glutamine, and asparagine), supplemented with 1mM pyruvate, 10mM HEPES, 100 IU/ml penicillin/streptomycin and 50µM 2-mercaptoethanol, and 10% dialysed FBS (Gibco), containing the indicated concentration of Asn, Asp (150µM), Glu (140µM), GlutaMAX (Thermo or Sigma)(2mM), except where mentioned otherwise. B cells were stimulated with agonistic anti-CD40 (5µg/ml, FGK45.4, functional grade, Miltenyi), recombinant IL-4 (1,10 or 50ng/ml, Peprotech), LPS (10µg/ml, Merck) or CpG (100nM, ODN1826, Miltenyi).

For proliferation experiments, cells were labelled with CellTrace Violet according to manufacturer's instructions (ThermoFisher) before stimulation. For stable isotope labelling, ^{15}N(amide)-asparagine (485896, Merck) (400µM), ^{15}N(amide)-glutamine (NLM-557, Cambridge Isotope Laboratories) (2mM), ^{15}N(amino)-glutamine (NLM-1016, Cambridge Isotope Laboratories) (2mM), or $^{13}C_5$-glutamine (CLM-1822, Cambridge Isotope Laboratories) (2mM) were used, replacing their unlabelled molecule in RPMI1640.

For nucleoside rescue experiment, adenosine (Fluorochem cat: F093333), thymidine (Fluorochem cat: F078885), uridine (Fluorochem cat: F078878), cytidine (Fluorochem cat: F226675) and guanosine (Merck, cat: G6264-5G) were prepared freshly in water and added to culture media at a final concentration of 30µM or 100µM.

Halofuginone hydrobromide (Bio-techne, cat no: 1993) was reconstituted in DMSO and used at 2nM and 5nM in the culture. Dimethyl 2-oxoglutarate (DM-OG) was purchased from Merck (cat no: 349631-5G) and added to the culture medium at 2mM and 4mM final concentrations.

Ex vivo lymph node slice culture

Inguinal lymph nodes (LNs) were harvested from B-WT or B-Asns mice immunised with NP-CGG subcutaneously on both flanks. They were then removed from surrounding fat by dissection and mild detergent wash (<1 sec) in 0.01% digitonin solution (Thermo Scientific) and embedded in 6% w/v low melting point agarose (Lonza) in 1x PBS. 300µm thick slices were cut using the Precisionary Compresstome® VF-210-0Z following manufacturer's instructions with a blade speed of 4 and oscillation of 6. The buffer tank was filled with ice cold PBS containing 1% Pen/Strep. Slices were removed from surrounding agarose and placed in a 24 well plate in 500µl of Asn-replete or Asn-free complete RPMI media in duplicate. LN slices were allowed to rest and equilibrate in the media for 1 hour at 37˚C and 5% CO2 before transferral into fresh media and incubation for 20hrs. Following culture, slices were collected, duplicate slices from same lymph nodes pooled, and slices disrupted into PBS containing 2% FBS and 2mM EDTA using the tip of an insulin syringe plunger to generate a cell suspension in a 96-well U bottom plate. Cells were then stained with viability dye and surface antigens. Following washes, cells were fixed in fresh 4% PFA (Cell Signalling) for 15 mins at 20°C and run on an Aurora flow cytometer (Cytek).

Flow cytometry

Spleens were dissociated by passing through 70µm cell strainers, and red cells lysed with ACK Lysis Buffer (Gibco). For Peyer's patch dissociation, a 70µm strainer (VWR) was also used. Single cell suspensions were incubated with Fixable Viability Dye eFluor™ 780 (eBioscience) or Zombie NIR (BioLegend) in PBS, followed by Fc Block (5 mins) and surface antibodies (30 mins on ice) in FACS buffer (PBS supplemented with 0.5% BSA and 2mM EDTA). For intracellular staining, cells were fixed in 4% paraformaldehyde at 20°C, then permeabilised with ice cold 90% methanol for 10 mins. To measure OPP ex vivo incorporation, cells were incubated in RPMI1640 with the indicated concentration of Asn, in the presence of 20µM OPP for 25 mins at 37°C. Click labelling was then performed with the Click-iT™ Plus OPP Alexa Fluor 647 Protein Synthesis Assay Kit (ThermoFisher, cat: C10458). Mitochondrial dye staining was performed with MitoTracker Green (100nM, Thermo) or MitoSOX (10µM, Thermofisher) for 30 mins in RPMI1640 at 37°C. NP binding was determined by incubation with NP-PE (Biosearch) for 30 mins at 4°C. Apoptosis was quantified by annexin V-FITC binding (Biolegend). The proliferation index was determined using the Proliferation module of FlowJo (BD).

Antibody (Catalogue number)	**Clone**	**Manufacturer**
Anti-GL-7 (144612)	GL-7	Biolegend
Anti-CD138(142504)	281-2	Biolegend
Anti-CD19 (115538)	6D5	Biolegend
Anti-IgD (405721)	11-26c-2a	Biolegend
Anti-CD38 (102718)	90	Biolegend
Anti-CXCR4 (146513)	L276F12	Biolegend
Anti-CD98 (128211)	RL388	Biolegend
Anti-IgG1 (406617)	RMG1-1	Biolegend
Anti-MHCII (107605)	M5/114.15.2	Biolegend
Anti-CD23 (101608)	B3B4	Biolegend
Anti-CD43 (12-0431-82)	eBioR2/60	ThermoFisher
Anti-CD86 (105031)	GL-1	Biolegend
Anti-B220 (103247)	RA3-6B2	Biolegend

Anti-IgM (406513)	RMM-1	Biolegend
Anti-CD21/35 (123409)	7E9	Biolegend
Anti-TACI (133403)	8F10	Biolegend
Anti-CD16/32 (Fc Block)	2.4G2	ThermoFisher
Anti-CXCR4 (741783)	2B11	BD Bioscience
Anti-CD38 (741955)	90	BD Bioscience
Anti-CD4 (100547)	RM4-5	Biolegend
Anti-PD-1 (135213)	29F.1A12	Biolegend
Anti-CXCR5 (145511)	L138D7	Biolegend
Anti-CD45.1 (110717)	A20	Biolegend
Anti-CD45.2 (109817)	104	Biolegend
Anti-CD3 (100215)	17A2	Biolegend
Anti-IRF4 (12-9858-82)	3E4	ThermoFisher
Anti-BCL6 (561525)	K112-91	BD Bioscience
Anti-CHOP (NB600-1335AF700)	9C8	Novus Bio

Immunofluorescence microscopy

Spleens were fixed overnight in Antigenfix (DiaPath) solution at 4°C. The next day, spleens were washed in PBS, followed by overnight incubation in 30% sucrose (in PBS) at 4°C for cryoprotection. On the following day, spleens were snap frozen in 100% methanol on dry ice and stored at -80°C until cryosectioning at 8-12µm thickness. Slides were then rehydrated in PBS at 20°C, then blocked in PBS containing 0.1% Tween-20, 10% goat serum, and 10% rat serum at RT for two hours. All primary antibody staining was performed overnight at 4°C or 1 hour at RT in PBS supplemented with 2% goat serum and 0.1% Tween-20. The following antibodies were used: anti-GL-7 (clone: GL-7), anti-CD45.2 (clone: 104) both from Biolegend.

To visualise protein synthesis in vivo, mice were immunised with SRBC using the enhanced protocol. At day 14, they were injected intraperitoneally with 1.5mg L-AHA (Thermo) and then 4 hours later 1mg OPP (Jena Bioscience) dissolved in 100µl PBS, or PBS alone as a negative control. Mice were sacrificed 1h later, and spleens were harvested for immunofluorescence analysis. L-AHA and OPP were detected by Click Chemistry using the Click-iT™ Plus L-AHA and then Click-iT™ Plus OPP Alexa Fluor™ 488 or 647 Protein Synthesis kits (Thermo) following the manufacturer's protocols.

Slides were mounted with Fluoromount G (Southern Biotech, cat: 0100-01) and imaged using a Zeiss LSM 980 equipped with an Airyscan 2 module.

Multiplexed Tissue Imaging using Cell DIVE

Formalin-fixed paraffin embedded (FFPE) human tonsil sections (5µm) were deparaffinised and rehydrated, and then permeabilised in 0.3% Triton X100 for 10 mins followed by washing in PBS for 5 mins. Antigen retrieval was performed in a Biocare NxGen decloaker by boiling the slides in a citrate-based antigen unmasking solution (Vector, #H3300) at pH 6, and then in a Tris-based antigen retrieval solution, containing 1×Tris, EDTA, 0.05% Tween20 and ddH2O (pH 9), for 20 mins at each step. The slides were blocked overnight in PBS solution containing 3% BSA (Merck, #A7906), 10% donkey serum (Bio-Rad, #C06SB), then incubated with human FcR Blocking Reagent (Miltenyi) at 1:100 at room temperature

for 1 hour. After washing in PBS, the slides were stained with DAPI (ThermoFisher), washed again, and cover slips were placed with mounting media (50% glycerol, [Sigma] and 4% propyl gallate [Sigma, #2370]).

All FFPE human tonsil slides were imaged using a GE Cell DIVE system. Firstly, a ScanPlan was performed by acquiring at 10× magnification so that regions of interest could be selected. This was then followed by imaging at 20× to acquire background autofluorescence and generate virtual H&E images. This background was subtracted from all subsequent rounds of staining.

All slides were decoverslipped in PBS before each staining round, which consisted of three antibodies applied in staining buffer (3% BSA in PBS). Unconjugated primary antibodies were used in the first round, incubated at 4°C overnight. The next day, slides were washed in 0.05% PBS-Tween 20, (Sigma, P9416) three times. AlexaFluor 488, 555 or 647 conjugated secondary antibodies were then added to the slides for an hour at room temperature. Directly conjugated antibodies were used in subsequent staining rounds, incubated at 4°C overnight. Antibody conjugation was performed in house for some of the antibodies using the antibody labelling kit (Invitrogen).

Fluorescent dye inactivation was performed by bleaching the slides with 0.1 M NaHCO3 (pH 10.9-11.3) (Sigma, S6297) and 3% H_2O_2 (Merck, #216763,) for 3 rounds (15 mins each) with a 1 min wash in PBS in between. The slides were then re-stained with DAPI for 2 mins before being washed in PBS. The bleached slides were imaged as the new background for subsequent subtraction.

Image analysis was performed in ImageJ. 225µm^2 region of interests (ROIs) were selected randomly in CD21$^-$ IgD$^-$ DZ GC, CD21$^+$ IgD$^-$ LZ GC and surrounding IgD$^+$ B cell follicle areas of individual GCs with representative DZ-LZ distribution. These ROIs were then inspected in the ASNS channel and mean fluorescence was calculated using the Measure function. Seven GCs from each tonsil were pooled for analysis, and a total of 21 GCs from 3 tonsils were quantified.

<u>Antibody list</u>

1. CD98 (#66883-1-Ig, Proteintech)
2. IgD (#324502, Biolegend)
3. ASNS (#14681-1-AP, Proteintech)
4. CD21 (#ab202692, abcam)
5. CD3 (#ab307335, abcam)
6. MZB1 (#NBP2-90320AF647, Novus)

3D Lattice SIM

Cultured B cells were transferred onto poly-L-lysine coated coverslips and incubated at 37°C for 10 minutes. Cells were subsequently fixed in 4% paraformaldehyde for 10 minutes at 37°C, before permeabilization and blocking 20°C for 30 minutes in PBS containing 0.2% Triton X-100, 10% goat serum and 10% rat serum. Staining with conjugated antibodies was then performed overnight at 4°C in PBS supplemented with 2% goat serum. Nuclear staining was carried out with DAPI diluted in PBS for 15 minutes at 20°C, prior to coverslip mounting with Fluoromount G (Southern Biotech, catalog no. 0100-01). Imaging was performed with

the Zeiss Elyra 7 lattice SIM using the 63× oil immersion objective and 15 phase SIM. SIM processing was then carried out on ZEN Black.

Image quantification of the mitochondrial network was performed using ImageJ software. Single cells were defined in individual Region of Interest (ROI) based on COX I signal. 3D mitochondrial morphological and network analysis was subsequently performed using an ImageJ plugin[48] with modified parameters: rolling (microns) 1.28 and gamma (0.90).

Extracellular flux analysis (SeaHorse)

Real-time oxygen consumption rates (OCR) and extracellular acidification rates (ECAR) were measured using a Seahorse XFe96 Extracellular Flux Analyzer (Agilent). Ex vivo isolated B cells from B-WT and B-Asns mice were stimulated (anti-CD40 at 5µg/ml and IL-4 at 10ng/ml) overnight at 10^6 cells per ml in a 24 well plate in the presence of varying concentrations of Asn. The next day, 2×10^5 B cells were plated on a poly-D lysine (Sigma)-coated XF96 cell culture microplate with 5-6 technical replicate wells and incubated at 37 °C for a minimum of 30 min in a CO_2-free incubator in assay medium (XF DMEM medium pH 7.40 supplemented with 2 mM L-glutamine, 1 mM pyruvate and 10 mM Glucose). Basal OCR and ECAR were measured, then followed by the MitoStress test, with oligomycin (1µM), fluorocarbonyl cyanide phenylhydrazone (FCCP, 2µM) and rotenone + antimycin A (0.5µM) (Agilent). Analyses were performed on Wave (Agilent).

ELISA

96 well EIA/RIA plates (Corning, cat: 3590) were coated with NP conjugated with BSA (NP_2 or $NP_{20>}$, cat: N5050XL-10 and cat: N-5050H-10, both from BioSearch) at 5µg/ml in bicarbonate/carbonate coating buffer overnight at 4°C. The next day, plates were washed with PBS and blocked with 5% skimmed milk in PBS for 2-2.5 hours at 37°C. Sera obtained from mice (NP-CGG-immunized day 14 subcutaneously or unimmunized control) were diluted in 1% skimmed milk (for IgG1 at 1:300, for IgM at 1:900) and added into blocked plates for exactly 1hr at 37°C. After several washes with PBS-Tween20 (0.05%), alkaline phosphatase-conjugated goat anti-mouse IgG1(Southern Biotech, cat: 1071-04) or IgM (Southern Biotech, cat: 1021-04) detection antibodies (at 1:2000 dilution) were incubated for exactly 1hr at 37°C. After the final washing step, plates were developed with alkaline phosphatase substrate (Sigma, cat: P7998-100ML) for 1hr with simultaneous reading on FLUOstar Omega plate reader every 5 mins.

Mass spectrometry

To extract molecules, cell were pelleted and washed twice with cold PBS and once with ice cold ammonium acetate (150mM, pH 7.3). The pellet was then resuspended in 1ml 80% LC-MS grade methanol/ultrapure water chilled on dry ice. The samples were vortexed three times on dry ice, and then centrifuged at 15,000×g for 5 mins. The initial supernatant was then transferred into a 1.8ml glass vial, and the pellet resuspended in 200µl 80% methanol as above, then centrifuged again at 15,000×g for 5 mins. The second supernatant was then combined with the first, dried at 4°C using a Centrivap (Conco), then stored at -80°C until analysis.

Dried metabolites were resuspended in 50% ACN:water and 1/10th was loaded onto a Luna 3µm NH_2 100A (150 × 2.0 mm) column (Phenomenex). The chromatographic separation was performed on a Vanquish Flex (Thermo Scientific) with mobile phases A (5mM NH_4AcO pH 9.9) and B (ACN) and a flow rate of 200µl/min. A linear gradient from 15% A to 95% A

over 18 min was followed by 7 min isocratic flow at 95% A and reequilibration to 15% A. Metabolites were detected with a Thermo Scientific Q Exactive mass spectrometer run with polarity switching (+3.5 kV/– 3.5 kV) in full scan mode with an m/z range of 70-975 and 140.000 resolution. Maven (v8.1.27.11) was used to quantify the targeted metabolites by area under the curve using expected retention time (as determined with pure standards) and accurate mass measurements (< 5 ppm). Values were normalized to cell number. Relative amounts of metabolites were calculated by summing up the values for all measured isotopologues of the targeted metabolites. Metabolite Isotopologue Distributions were corrected for natural ^{15}N abundance. Metabolite and transcriptome data were analysed using MetaboAnalyst[49] and statistical analysis was performed in R.

Western blotting

Cells were lysed on ice in RIPA buffer (Merck) supplemented with protease and phosphatase inhibitors (cOmplete™ ULTRA Tablets and PhosSTOP™, Roche) for 30mins with frequent vortexing, and then centrifuged at 15,000×g for 15mins at 4°C and the supernatant recovered. Protein was quantified using the BCA method (Pierce, Thermo). Samples were denatured in Laemmli buffer (BioRad) containing 10% β-mercaptoethanol at 90°C for 5 mins then transferred to ice, before running on a 4-15% gel (Mini-PROTEAN TGX Precast Gels, BioRad). Protein was transferred onto PVDF membranes (BioRad), which were blocked in 2.5% skimmed milk for 1h, and then stained with the primary antibody diluted in 2.5% BSA/0.05% TBS-Tween 20 at 4°C overnight.

Following washing, membranes were then incubated with horseradish peroxidase (HRP)-conjugated goat anti-rabbit secondary antibody in 2.5% milk/0.05% TBS-Tween 20 for 1h at RT. Chemiluminescence was used to detect the secondary antibody (Anti-rabbit IgG, HRP-linked Antibody #7074 and SuperSignal™ West Pico PLUS Chemiluminescent Substrate, ThermoFisher).

Antibody (Catalogue number)	**Dilution**	**Clone**	**Manufacturer**
DHODH (14877-1-AP)	1:1000	Polyclonal	Proteintech
ASNS (14681-1-AP)	1:2000	Polyclonal	Proteintech
CHOP (2895)	1:1000	L63F7	Cell Signaling
Phospho-4E-BP1 (236B4)	1:500	Monoclonal	Cell Signaling
ATF4 (11815)	1:500	D4B8	Cell Signaling
Vinculin (13901)	1:1000	E1E9V	Cell Signaling
β-actin (4970)	1:2000	13E5	Cell Signaling
Phospho-CAD (12662)	1:2000	Polyclonal	Cell Signaling
ATIC (ab188321)	1:500	EPR13243-53	Abcam
Phospho-eIF2a (9721)	1:500	Polyclonal	Cell Signaling

Quantitative PCR

Cells were washed in PBS and lysed in RLT Plus buffer (Qiagen) supplemented with 1% β-mercaptoethanol. RNA extraction was performed according to manufacturer's instructions using an RNeasy Plus Mini Kit (Qiagen). Reverse transcription was performed using the High Capacity RNA-to-cDNA Kit (Thermo). Quantitative qPCR was performed using Taqman Probes (Thermo). Relative expression was calculated with reference to *Ubc*.

List of probes used:

Gene	Taqman ProbeID
Asns	Mm00803785_m1
Ubc	Mm02525934_g1
Atf4	Mm00515325_g1
Dhodh	Mm00498393_m1
Adsl	Mm00507759_m1
Umps	Mm00801991_m1
Cad	Mm01216345_m1
Ppat	Mm00549096_m1
Atic	Mm00546563_m1
Pfas	Mm01325237_m1
Got2	Mm00494703_m1
Zbtb1	Mm01281881_m1

RNA sequencing

RNA was quantified using RiboGreen (Invitrogen) on the FLUOstar OPTIMA plate reader (BMG Labtech) and the size profile and integrity analysed on a 2200 or 4200 TapeStation (Agilent, RNA ScreenTape). RIN estimates were between 9.3 and 9.7. Input material was normalised to 100 ng prior to library preparation. Polyadenylated transcript enrichment and strand specific library preparation was completed using NEBNext Ultra II mRNA kit (NEB) following manufacturer's instructions. Libraries were amplified (17 cycles) on a Tetrad (Bio-Rad) using in-house unique dual indexing primers (based on DOI: 10.1186/1472-6750-13-104). Individual libraries were normalised using Qubit, and the size profile was analysed on a 2200 or 4200 TapeStation. Individual libraries were normalised and pooled together accordingly. The pooled library was diluted to ~10nM for storage. The 10nM library was denatured and further diluted prior to loading on the sequencer. Paired end sequencing was performed using a NovaSeq6000 platform (Illumina, NovaSeq 6000 S2/S4 reagent kit, 300 cycles).

Transcripts were counted using *Salmon*, and differential gene expression and pathway analysis performed using the R packages *DESeq2* and *fgsea*.

Statistical analysis
The use of the statistical tests is indicated in the respective figure legends, with the error bars indicating the mean ± S.E.M. P values ≤ 0.05 were considered to indicate significance. Analyses were performed with GraphPad Prism v9-10 or R 4.1. No statistical methods were used to pre-determine sample sizes, but our sample sizes are similar to those reported in previous publications. The distribution of data was determined using normality testing to determine appropriate statistical methodology, or otherwise assumed to be normally distributed. For in vivo experiments we matched the age of the mice in experimental batches, but other modes of randomization were not performed. Data collection and analysis were not performed blind to the conditions of the experiments in most of the experiments. In some experiments, the R package *Batchma* was used for batch correction.

Data availability
RNA sequencing data has been uploaded to GEO under accession number GSE228845.

Code availability
This paper does not report novel code.

Author contributions
Y.Y., E.M., and A.C. conceived and designed the study. Y.Y., E.M., K.B., H.A., Z.Y.W, R.M, J.F., M.A, and B.K. performed experiments. A.C. and E.M. analysed metabolomic and transcriptional data. Y.Y. performed image analysis. C.B., M.C. and S.J.D. provided resources. Y.Y. and A.C. wrote the manuscript and A.C. supervised the study.

Acknowledgements
We thank Johanna ten Hoeve-Scott (UCLA Metabolomics Center, United States) for performing metabolomics studies. We thank Sarah Lamble (Oxford Genomics Centre) for performing RNA sequencing studies. We thank Kristina Zec, Lion Uhl, Julia Johnstone, and Mariana Borsa for technical assistance. We also thank Jonathan Webber for flow sorting and the BSU staff for support (Kennedy Institute of Rheumatology, University of Oxford). We would like to acknowledge the Oxford-ZEISS Centre of Excellence in Biomedical Imaging. Funding for this work was provided by the Wellcome Trust (211072/Z/18/Z) and Cancer Research UK/Versus Arthritis (C70663/A29547) to A.C., the Kennedy Trust for Rheumatology Research to Y.Y.

For the purpose of open access, the author has applied a CC BY-ND public copyright license to any Author Accepted Manuscript version arising from this submission. The computational aspects of this research were supported by the Wellcome Trust Core Award Grant Number 203141/Z/16/Z and the NIHR Oxford BRC. The views expressed are those of the author(s) and not necessarily those of the NHS, the NIHR or the Department of Health. 3D SIM imaging was supported by a Medical Research Council Grant MC_PC_MR/X012069/1. We acknowledge the contribution to this study made by the Oxford Centre for Histopathology Research and the Oxford Radcliffe Biobank, which are funded by the University of Oxford, the Oxford CRUK Cancer Centre, the NIHR Oxford Biomedical Research Centre (BRC) (Molecular Diagnostics Theme/Multimodal Pathology Subtheme and the NIHR CRN Thames Valley network. Oxford Radcliffe Biobank (ORB) research tissue bank ethics, reference 19/SC/0173 for tonsil sections.

References

1. Victora, G. D. & Nussenzweig, M. C. Germinal Centers. *Annu. Rev. Immunol.* **40**, 413–442 (2022).
2. Boothby, M. & Rickert, R. C. Metabolic Regulation of the Immune Humoral Response. *Immunity* **46**, 743–755 (2017).
3. Chen, D. *et al.* Coupled analysis of transcriptome and BCR mutations reveals role of OXPHOS in affinity maturation. *Nat. Immunol.* 1–10 (2021) doi:10.1038/s41590-021-00936-y.
4. Weisel, F. J. *et al.* Germinal center B cells selectively oxidize fatty acids for energy while conducting minimal glycolysis. *Nat. Immunol.* **21**, 331–342 (2020).
5. Urbanczyk, S. *et al.* Mitochondrial respiration in B lymphocytes is essential for humoral immunity by controlling the flux of the TCA cycle. *Cell Rep.* **39**, 110912 (2022).
6. Luo, W. *et al.* SREBP signaling is essential for effective B cell responses. *Nat. Immunol.* 1–12 (2022) doi:10.1038/s41590-022-01376-y.
7. Sharma, R. *et al.* Distinct metabolic requirements regulate B cell activation and germinal center responses. *Nat. Immunol.* 1–12 (2023) doi:10.1038/s41590-023-01540-y.
8. Cho, S. H. *et al.* Germinal centre hypoxia and regulation of antibody qualities by a hypoxia response system. *Nature* **537**, 234–238 (2016).
9. Geiger, R. *et al.* L-Arginine Modulates T Cell Metabolism and Enhances Survival and Anti-tumor Activity. *Cell* **167**, 829-842.e13 (2016).

10. Ron-Harel, N. *et al.* Mitochondrial Biogenesis and Proteome Remodeling Promote One-Carbon Metabolism for T Cell Activation. *Cell Metab.* **24**, 104–117 (2016).
11. Sinclair, L. V. *et al.* Control of amino-acid transport by antigen receptors coordinates the metabolic reprogramming essential for T cell differentiation. *Nat. Immunol.* **14**, 500–508 (2013).
12. Fernández-García, J. *et al.* CD8+ T cell metabolic rewiring defined by scRNA-seq identifies a critical role of ASNS expression dynamics in T cell differentiation. *Cell Rep.* **41**, (2022).
13. Wu, J. *et al.* Asparagine enhances LCK signalling to potentiate CD8 + T-cell activation and anti-tumour responses. *Nat. Cell Biol.* **23**, 75–86 (2021).
14. Hope, H. C. *et al.* Coordination of asparagine uptake and asparagine synthetase expression modulates $CD8^+$ T cell activation. *JCI Insight* **6**, (2021).
15. Gnanaprakasam, J. N. R. *et al.* Asparagine restriction enhances CD8+ T cell metabolic fitness and antitumoral functionality through an NRF2-dependent stress response. *Nat. Metab.* 1–17 (2023) doi:10.1038/s42255-023-00856-1.
16. Kelly, B. & Pearce, E. L. Amino Assets: How Amino Acids Support Immunity. *Cell Metab.* S1550413120303119 (2020) doi:10.1016/j.cmet.2020.06.010.
17. Eraslan, Z., Papatzikas, G., Cazier, J.-B., Khanim, F. L. & Günther, U. L. Targeting Asparagine and Serine Metabolism in Germinal Centre-Derived B Cells Non-Hodgkin Lymphomas (B-NHL). *Cells* **10**, 2589 (2021).
18. Parsa, S. *et al.* The serine hydroxymethyltransferase-2 (SHMT2) initiates lymphoma development through epigenetic tumor suppressor silencing. *Nat. Cancer* **1**, 653–664 (2020).
19. D'Avola, A. *et al.* PHGDH is required for germinal center formation and is a therapeutic target in MYC-driven lymphoma. *J. Clin. Invest.* **132**, e153436 (2022).
20. Grima-Reyes, M. *et al.* Tumoral microenvironment prevents de novo asparagine biosynthesis in B cell lymphoma, regardless of ASNS expression. *Sci. Adv.* **8**, eabn6491 (2022).
21. Cantor, J. *et al.* CD98hc facilitates B cell proliferation and adaptive humoral immunity. *Nat. Immunol.* **10**, 412–419 (2009).
22. Dieterich, D. C., Link, A. J., Graumann, J., Tirrell, D. A. & Schuman, E. M. Selective identification of newly synthesized proteins in mammalian cells using bioorthogonal noncanonical amino acid tagging (BONCAT). *Proc. Natl. Acad. Sci.* **103**, 9482–9487 (2006).
23. Painter, M. W. *et al.* Transcriptomes of the B and T Lineages Compared by Multiplatform Microarray Profiling. *J. Immunol.* **186**, 3047–3057 (2011).
24. Müller-Winkler, J. *et al.* Critical requirement for BCR, BAFF, and BAFFR in memory B cell survival. *J. Exp. Med.* **218**, e20191393 (2020).
25. Lomelino, C. L., Andring, J. T., McKenna, R. & Kilberg, M. S. Asparagine synthetase: Function, structure, and role in disease. *J. Biol. Chem.* **292**, 19952–19958 (2017).
26. Hobeika, E. *et al.* Testing gene function early in the B cell lineage in mb1-cre mice. *Proc. Natl. Acad. Sci. U. S. A.* **103**, 13789–13794 (2006).
27. Akiyama, T., Kobayashi, K., Higashikage, A., Sato, J. & Yoshinaga, H. CSF/plasma ratios of amino acids: Reference data and transports in children. *Brain Dev.* **36**, 3–9 (2014).
28. Sullivan, L. B. *et al.* Aspartate is an endogenous metabolic limitation for tumour growth. *Nat. Cell Biol.* 1–12 (2018) doi:10.1038/s41556-018-0125-0.
29. Crawford, J. & Cohen, H. J. The essential role of L-glutamine in lymphocyte differentiation in vitro. *J. Cell. Physiol.* **124**, 275–282 (1985).
30. Belanger, M. C. *et al.* Acute Lymph Node Slices Are a Functional Model System to Study Immunity Ex Vivo. *ACS Pharmacol. Transl. Sci.* **4**, 128–142 (2021).

31. Harding, H. P. *et al.* An Integrated Stress Response Regulates Amino Acid Metabolism and Resistance to Oxidative Stress. *Mol. Cell* **11**, 619–633 (2003).
32. Pakos-Zebrucka, K. *et al.* The integrated stress response. *EMBO Rep.* **17**, 1374–1395 (2016).
33. Williams, R. T. *et al.* ZBTB1 Regulates Asparagine Synthesis and Leukemia Cell Response to L-Asparaginase. *Cell Metab.* **31**, 852-861.e6 (2020).
34. Sundrud, M. S. *et al.* Halofuginone Inhibits TH17 Cell Differentiation by Activating the Amino Acid Starvation Response. *Sci. N. Y. NY* **324**, 1334–1338 (2009).
35. Sugimoto, K. *et al.* A clinically attainable dose of L-asparaginase targets glutamine addiction in lymphoid cell lines. *Cancer Sci.* **106**, 1534–1543 (2015).
36. Yazicioglu, Y. F. *et al.* Dynamic mitochondrial transcription and translation in B cells control germinal center entry and lymphomagenesis. *Nat. Immunol.* (2023) doi:10.1038/s41590-023-01484-3.
37. Spinelli, J. B. & Haigis, M. C. The multifaceted contributions of mitochondria to cellular metabolism. *Nat. Cell Biol.* **20**, 745–754 (2018).
38. Rawls, J., Knecht, W., Diekert, K., Lill, R. & Löffler, M. Requirements for the mitochondrial import and localization of dihydroorotate dehydrogenase. *Eur. J. Biochem.* **267**, 2079–2087 (2000).
39. Scherer, S. *et al.* Pyrimidine de novo synthesis inhibition selectively blocks effector but not memory T cell development. *Nat. Immunol.* **24**, 501–515 (2023).
40. Torrence, M. E. *et al.* The mTORC1-mediated activation of ATF4 promotes protein and glutathione synthesis downstream of growth signals. *eLife* **10**, e63326 (2021).
41. Wang, W. & Zou, W. Amino Acids and Their Transporters in T Cell Immunity and Cancer Therapy. *Mol. Cell* **80**, 384–395 (2020).
42. Jones, M. A. *et al.* Discovering New Lipidomic Features Using Cell Type Specific Fluorophore Expression to Provide Spatial and Biological Specificity in a Multimodal Workflow with MALDI Imaging Mass Spectrometry. *Anal. Chem.* **92**, 7079–7086 (2020).
43. Rossi, M. *et al.* PHGDH heterogeneity potentiates cancer cell dissemination and metastasis. *Nature* **605**, 747–753 (2022).
44. Ben-Sahra, I., Howell, J. J., Asara, J. M. & Manning, B. D. Stimulation of de Novo Pyrimidine Synthesis by Growth Signaling Through mTOR and S6K1. *Science* **339**, 1323–1328 (2013).
45. Ben-Sahra, I., Hoxhaj, G., Ricoult, S. J. H., Asara, J. M. & Manning, B. D. mTORC1 induces purine synthesis through control of the mitochondrial tetrahydrofolate cycle. *Sci. N. Y. NY* **351**, 728–733 (2016).
46. Dominguez-Sola, D. *et al.* The proto-oncogene MYC is required for selection in the germinal center and cyclic reentry. *Nat. Immunol.* **13**, 1083 EP-.
47. Cato, M. H., Yau, I. W. & Rickert, R. C. Magnetic-based purification of untouched mouse germinal center B cells for ex vivo manipulation and biochemical analysis. *Nat. Protoc.* **6**, 953–960 (2011).
48. Chaudhry, A., Shi, R. & Luciani, D. S. A pipeline for multidimensional confocal analysis of mitochondrial morphology, function, and dynamics in pancreatic β-cells. *Am. J. Physiol. Endocrinol. Metab.* **318**, E87–E101 (2020).
49. Xia, J., Sinelnikov, I. V., Han, B. & Wishart, D. S. MetaboAnalyst 3.0—making metabolomics more meaningful. *Nucleic Acids Res.* **43**, W251–W257 (2015).